Numerical Methods in Condensed Matter Physics

by

Maksim A Skorobogatiy

Submitted to the Department of Electrical Engineering and Computer Science
in partial fulfillment of the requirements for the degree of

Master of Science in Electrical Engineering and Computer Science

at the

MASSACHUSETTS INSTITUTE OF TECHNOLOGY

June 2000

Author .....
Department of Electrical Engineering and Computer Science
January, 2000

Certified by .....
John D. Joannopoulos
Francis Wright Davis Professor of Physics
Thesis Supervisor

Accepted by .....
Arthur C. Smith
Chairman, Department Committee on Graduate Students

Numerical Methods in Condensed Matter Physics

by

Maksim A Skorobogatiy

Submitted to the Department of Electrical Engineering and Computer Science
on January, 2000, in partial fulfillment of the
requirements for the degree of
Master of Science in Electrical Engineering and Computer Science

Abstract

Condensed Matter Physics is a reach source of theoretical as well as computational problems each of them frequently requiring an individual approach and method of solution. This thesis is based on a set of research projects conducted by the author at MIT and addresses the computational methods for solving a set of problems in Condensed Matter Physics involving nin-linear coupled Partial Differential Equations (PDE's). First, finite difference numerical schemes for solving coupled nonlinear PDE's with non-trivial boundary conditions are discussed on the example of folding of viscous filaments in two dimensions. This problem is relevant to Soft Condensed Matter Physics. Second, computational methods explicitly employing some functional basis into which trial solutions are expended are considered on the example of a structure of the electro-magnetic modes in a material with a spatially periodic dielectric constant (a so called photonic crystal). Finally, electro-magnetic modes in a photonic crystal undergoing rigid vibrations are investigated leading to a formulation and solution of a generalized eigen value problem. The last problem is relevant to the field of Photonic Band Gap materials and Optical Devices.

Thesis Supervisor: John D. Joannopoulos
Title: Francis Wright Davis Professor of Physics

Acknowledgments

To all my Mentors and Benefactors. Special tribute to my Mother and Father, and to my intellectual Inspirers Prof. J.D. Joannopoulos, Prof. L. Mahadevan, my deeply respectable friend and mentor Prof. Martin Zuckermann, and always enthusiastic and keen Prof. Hong Guo.

Contents

List of Figures

Chapter 1

Introduction

Condensed Matter Physics is a rich source of theoretical as well as computational problems each of them frequently requiring an individual approach and method of solution. This thesis is based on a set of research projects conducted by the author at MIT and addresses the computational methods for solving a set of problems in Condensed Matter Physics involving non-linear coupled Partial Differential Equations (PDE's). First, finite difference numerical schemes for solving coupled nonlinear PDE's with non-trivial boundary conditions are discussed for the example of folding of viscous filaments in two dimensions. This problem is relevant to Soft Condensed Matter Physics. Second, computational methods explicitly employing some functional basis into which trial solutions are expended are considered for the example of a structure of the electro-magnetic modes in a material with a spatially periodic dielectric constant (a so called photonic crystal). Finally, electro-magnetic modes in a photonic crystal undergoing rigid vibrations are investigated leading to a formulation and solution of a generalized eigen value problem. The last problem is relevant to the field of Photonic Band Gap materials and Optical Devices.

This thesis is organized as follows:

Chapter one covers the ideas and methods of implementation behind the two common approaches for solving systems of PDE's. The first approach described is a finite difference method (method without an explicit functional basis). Finite difference approximation of spatial and temporal derivatives, stability analysis and simple bound-

ary conditions implementation is considered. Finally, imposing non-trivial boundary conditions such as linear and nonlinear constraints is discussed by employing a non-linear Newton relaxation algorithm. The described methods are demonstrated for the example of a heat transfer problem in a low-temperature experimental setup. The second approach covered in the chapter is a method of solving PDE's explicitly using some functional basis into which a trial solution is expanded. It is shown how this method reduces a set of PDE's to a set of non-linear multidimensional algebraic equations. Frequently, however a transformed problem is easier to solve than an original one. For example, in the case of wave propagation equations a transformed problem constitutes a standard eigen value problem which allows many effective solution techniques. This method of solving PDE's is demonstrated on the example of finding electro-magnetic modes of a stationary photonic crystal.

Chapter two of the thesis is entitled "Folding of Viscous Filaments in Two Dimensions". This problem involves solving a set of hydrodynamical nonlinear coupled PDE's with non-trivial boundary conditions in space and time. Done under the supervision of Prof. L. Mahadevan (Dept. of Mechanical Engineering) this part employs a finite difference scheme with a Newton relaxation method to impose the non-trivial boundary conditions.

Chapter three of the thesis is entitled "Photonic Crystals Undergoing Rigid Vibrations". Numerical methods explicitly employing some functional basis set are demonstrated in this chapter by expanding a trial solution for the electro-magnetic modes of a photonic crystal into the planewave basis functions. Finding of the energy bands of a stationary photonic crystal, thus, involves a determination of the *eigenvectors* and *eigenvalues* of some Hermitian matrix. This problem is standard and allows many efficient solutions. When a photonic crystal is put in rigid vibration determining the energy bands becomes a generalized problem of finding *eigenvectors* and *eigenmatrices* of some algebraic relation. If the perturbation of a photonic crystal from its stationary state is small, the *eigenmatrices* can be found using a multidimensional Newton algorithm with stationary *eigenvectors* and *eigenvalues* as initial guesses. This part of a thesis was done under the supervision of Prof. J.D.

Joannopoulos (Dept. of Physics).

Now we proceed with describing the ideas behind the two popular approaches in solving PDE's for the example of the problem of heat conduction in slender rods and the problem of wave propagation in periodic dielectrics. These problems involve two very different classes of PDE's frequently encountered in physical and engineering problems. We discuss in details the methodology as well as the applicability of each of the method in revealing the spatial and temporal structure of the solutions of these equations. An excellent introduction into the numerical methods for solving PDE's as well as into the numerical methods in general can be found in [1, 2]. We start with describing a finite difference approach for solving PDE's (also known as a method without an explicit functional basis). This method will be demonstrated on the example of a problem of heat conduction in a slender rod. After that, we are going to demonstrate another method of solving PDE's that explicitly assumes some functional basis into which trial solutions are expanded. This method will be demonstrated on the example of the electro-magnetic states in the periodic dielectric materials.

1.1 Finite difference methods for solving PDE's

Many physical problems involve a time evolution as well as a spatial distribution of a particular quantity such as temperature, current, etc. One common problem of this type involves a study of the temperature equilibration and temperature profiles in a block of some material. This problem is of a wide applicability ranging from the design of the experimental setups in low temperature physics to the study of the heat shields in avionics. In this section we discuss a simple version of this problem in detail. First, we discuss the form of the equations involved. Next we show how these equations can be solved on a real space grid, particularly, we pay special attention to the choice of the finite difference operators, implementation of the boundary conditions and conditions of stability of a particular finite difference scheme. Finally, the way of imposing non-trivial constraints using a multidimensional nonlinear Newton method

is discussed.

Consider a one dimensional model in which a rod of a thermally conducting material with thermal conductivity κ and a heat capacitance per unit length C has one end suspended in a thermostat at temperature T_0 while the other end is protruding freely in a media of low thermal conductivity such as air (see figure 1-1 b)). This model can be used to simulate a heat flow in a low temperature experimental setup where a hollow rod (containing wiring) with a metal container at the end (hosting different samples) is placed with its one end into a liquid nitrogen $T_0 = 77K$ or a liquid helium $T_0 = 4K$, while the other end of the rod is sticking out into the air at room temperature $T_R = 277K$ (see figure 1-1 a)). A question of interest here is about the magnitude of a heat flux from the air into the open end of the rod. We will describe the finite difference method of solving PDE's on the example of the equations governing the heat flow in this particular system.

An equation governing the heat flow in a rod-like one dimensional geometry described above can be derived from thermodynamics and has a form

$$\kappa \frac{\partial^2 T(x,t)}{\partial x^2} = C \frac{\partial T(x,t)}{\partial t} \tag{1.1}$$

where $T(x,t)$ is a temperature profile inside a rod at time t and such a profile is defined on a spatial interval $x \in [0, L]$. First we note that PDE 1.1 is second order in space and first order in time. Thus, to solve this equation, an initial temperature profile $T(x,0)$ at time $t = 0$ should be specified, as well as the two spatial boundary conditions should be specified at each point of time. At the lower end $x = L$ the boundary condition imposes the temperature of the end to be the one of the thermostat

$$T(x,t)|_{x=L} = T_0. \tag{1.2}$$

At the end sticking into the air, one can use a so called Newton boundary condition stating that the heat flow from the air into the rod is linearly proportional to the temperature difference between the temperature of the air and the temperature of

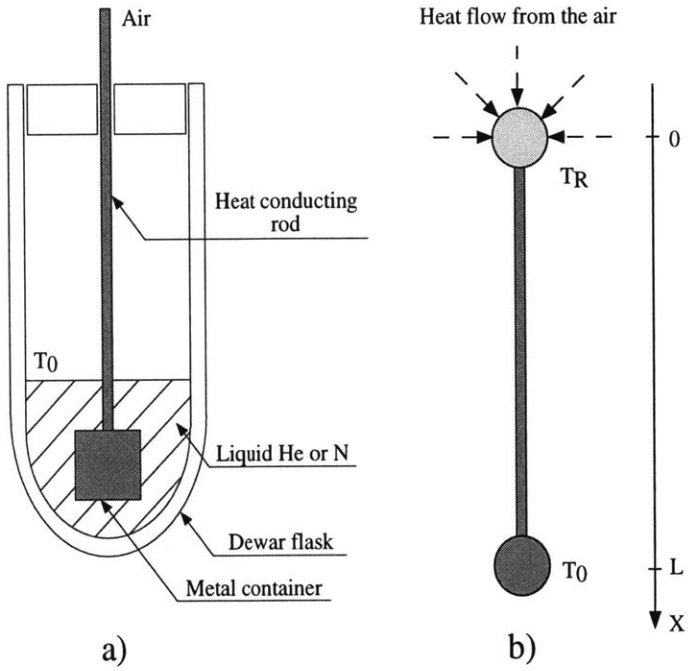

Figure 1-1: a) A sketch of a common experimental low temperature setup used in many variations to study physical phenomena at low temperatures. A long hollow rod containing wiring has a metal container at one of its ends. This container serves as a holder for the samples under study. Container is submerged into a coolant which is usually either a liquid helium or a liquid nitrogen. The other end of the rod is sticking out into the air ; b) To model a heat flow from the air into the coolant through the center rod we consider a one dimensional abstraction to the experimental setup in which the rod is considered to be a uniform cylinder with one of its ends sticking out in the air while the other end is kept at a constant temperature T_0.

the end of the rod. Thus, the second boundary condition at the other end is given by

$$\frac{\partial T(x,t)}{\partial x}|_{x=0} = -\eta(T_R - T(0,t)). \tag{1.3}$$

To proceed further, we rescale different parameters of the problem making them dimensionless. We define $\bar{x} = \frac{x}{L}$, $\bar{t} = \frac{t\kappa}{CL^2}$, $\bar{\eta} = \eta L$. Substituting thus defined dimensionless variables into equations 1.1, 1.2, 1.3 and dropping the bars we have the following rescaled equations and boundary conditions

$$\begin{cases} \frac{\partial^2 T(x,t)}{\partial x^2} &= \frac{\partial T(x,t)}{\partial t}, \\ T(x,t)|_{x=1} &= T_0, \\ \frac{\partial T(x,t)}{\partial x}|_{x=0} &= -\eta(T_R - T(0,t)). \end{cases} \tag{1.4}$$

where now $T(x,t)$ is a temperature profile defined on an interval $x \in [0,1]$ at time t.

The fist problem which one faces trying to solve equation 1.4 numerically is dealing with a continuous two dimensional variable $T(x,t)$. As computers operate only with discrete variables we either have to approximate $T(x,t)$ on some spatial-temporal grid or introduce a suitable set of continuous basis functions into which $T(x,t)$ can be decomposed with a discrete set of coefficients. In practice, both methods are used. In the following section we will describe methods that approximate $T(x,t)$ on a spatial-temporal grid and in the section after that we will address methods explicitly employing some functional basis set in which trial solutions are expanded.

1.1.1 Defining the finite difference operators

We define $T(i,j)$ to be a discrete function specified on a uniformly spaced grid $i \in [1,...,N]$, $j \geq 0$ covering a spatial dimension with the intervals of $dx = \frac{1}{N-1}$, and covering a temporal dimension with the intervals of dt. To solve equation 1.4 numerically we want to reformulate a problem in terms of finding a discrete function $T(i,j)$ as an approximation to a continuous function $T(x,t)$. To proceed further we have to make sense of the spatial derivatives $\frac{\partial^2 T(x,t)}{\partial x^2}$, $\frac{\partial T(x,t)}{\partial x}$ as well as a temporal derivative $\frac{\partial T(x,t)}{\partial t}$ of equation 1.4 in terms of the values of a grid function $T(i,j)$. As

soon as such a correspondence is established we can solve thus discretized equations to find $T(i,j)$. One expects for a discretized version of equation 1.4 to have a form

$$\begin{cases} \frac{\partial^2 T(i,j)}{\partial i^2} &= \frac{\partial T(i,j)}{\partial j}, \\ T(i,j)|_{i=N} &= T_0, \\ \frac{\partial T(i,j)}{\partial i}|_{i=1} &= -\eta(T_R - T(0,j)). \end{cases} \tag{1.5}$$

where $\frac{\partial^2 T(i,j)}{\partial i^2}$, $\frac{\partial T(i,j)}{\partial i}$, and $\frac{\partial T(i,j)}{\partial j}$ are the discretized analogs of the derivatives $\frac{\partial^2 T(x,t)}{\partial x^2}$, $\frac{\partial T(x,t)}{\partial x}$, and $\frac{\partial T(x,t)}{\partial t}$, chosen in such a way that a solution of equation 1.5 matches exactly a solution of equation 1.4 at the grid points. Values at the non-grid points can be interpolated using $T(i,j)$ to retrieve a continuous solution $T(x,t)$.

As the spatial and temporal discretization intervals dx, dt become smaller and smaller (the number of grid points in each dimension becomes larger and larger) one can hope intuitively that if the finite difference scheme is chosen correctly the representation of $T(x,t)$ in terms of $T(i,j)$ and interpolation into the non-grid intervals should become increasingly more accurate. In practice, however, any finite difference scheme 1.5 gives a solution matching an exact solution of equation 1.4 at the grid points only approximately, which leads to a necessity of a strict control over the errors of discretization (see a section on stability).

In the following, to approximate derivatives of the field $T(x,t)$ we use the values of $T(i,j)$ at the grid points (i,j) as if $T(i,j)$ were exactly equal to the $T(x,t)$ at such points $x = idx, \quad t = jdt$. In other words, we can intuitively assume that in the limit of $dx \to 0, \quad dt \to 0$ a solution $T(i,j)$ of a discretized equation 1.5 does equal exactly to an exact solution $T(x,t)$ of equation 1.4 at $x = idx, \quad t = jdt$. If this assumption is correct (which can be proved to be correct for most of the ordinary PDE's) then we can use grid values of $T(i,j)$ to define the discretized derivatives of $T(x,t)$ in equation 1.5.

To do that we first use a Taylor series to express derivatives of $T(x,t)$ at any (x,t)

in terms of the $T(x,t)$ grid values. For example, for a second order spatial derivative

$$\frac{\partial^2 T(x,t)}{\partial x^2} = \frac{T(x+dx,t) - 2T(x,t) + T(x-dx,t)}{dx^2} + O(dx^2). \tag{1.6}$$

If one desires to use a more accurate approximation to the second order spatial derivative of $T(x,t)$ one can use more grid points thus, for example, up to the forth order in dx

$$\frac{\partial^2 T(x,t)}{\partial x^2} = \frac{-\frac{1}{12}T(x+2dx,t) + \frac{4}{3}T(x+dx,t) - \frac{5}{2}T(x,t) + \frac{4}{3}T(x-dx,t) - \frac{1}{12}T(x-2dx,t)}{dx^2} + O(dx^4). \tag{1.7}$$

In principle, one can design the grid point derivative approximations of any order of accuracy, such approximations are well known and tabulated in different sources [2]. A word of caution here is that using very accurate approximations of the derivatives will pay off only if all the derivative approximations in equation 1.5 are carefully balanced to the same order of accuracy with all the other terms in a PDE itself as well as in the boundary conditions.

Next, we define the discretized derivatives in equation 1.5 by substituting the grid values of $T(x,t)$ in equations 1.6,1.7 by the grid values $T(i,j)$ of the finite difference solution of equation 1.5. So, for example, to the second and forth order in dx

$$\begin{aligned} \frac{\partial^2 T(i,j)}{\partial i^2} &= \frac{T(i+1,j) - 2T(i,j) + T(i-1,j)}{dx^2} + O(dx^2), \\ \frac{\partial^2 T(i,j)}{\partial i^2} &= \frac{-\frac{1}{12}T(i+2,j) + \frac{4}{3}T(i+1,j) - \frac{5}{2}T(i,j) + \frac{4}{3}T(i-1,j) - \frac{1}{12}T(i-2,j)}{dx^2} + O(dx^4). \end{aligned} \tag{1.8}$$

By analogy, to the first and second order in dt

$$\begin{aligned} \frac{\partial T(i,j)}{\partial j} &= \frac{T(i,j+1) - T(i,j)}{dt} + O(dt), \\ \frac{\partial T(i,j)}{\partial j} &= \frac{T(i,j+1) - T(i,j-1)}{2dt} + O(dt^2). \end{aligned} \tag{1.9}$$

Finally, choosing say a second order in accuracy operator $\frac{\partial^2 T(i,j)}{\partial i^2}$ and a first order in accuracy temporal operator $\frac{\partial T(i,j)}{\partial j}$ and disregarding the $O(dx^2)$ and $O(dt)$ discretiza-

tion errors we arrive to the following form of the discretized heat flow equation 1.5

$$\frac{T(i+1,j)-2T(i,j)+T(i-1,j)}{dx^2}=\frac{T(i,j+1)-T(i,j)}{dt}. \tag{1.10}$$

1.1.2 Boundary conditions

As was mentioned previously, equation 1.4 is second order in space and first order in time PDE which requires a specification of the two spatial and one temporal boundary conditions. In fact, the boundary conditions are intimately interlaced with a choice of the finite difference operators. To appreciate this fact we try to rewrite equation 1.10 in a matrix form (which has to be done when solving it numerically). Notice, that for all the "true inside" points $i \in [2, N-1]$ and for any $j \geq 0$ all the finite difference operators in equation 1.10 are well defined. However, for the points close to the spatial boundaries $i = 1$ and $i = N$ spatial second order finite difference operator $\frac{T(i+1,j)-2T(i,j)+T(i-1,j)}{dx^2}$ is not defined as its values become $\frac{T(2,j)-2T(1,j)+T(0,j)}{dx^2}$ and $\frac{T(N+1,j)-2T(N,j)+T(N-1,j)}{dx^2}$ for $i = 1$ and $i = N$ correspondingly. These operators are not defined as they contain values $T(0,j)$ and $T(N+1,j)$ that are not defined on the considered domain $i \in [1, N]$. However, "luckily" we need these two "outside" points anyway to specify the two spatial boundary conditions. As far as the temporal boundary condition is concerned it is trivially specified by fixing initial temperature distribution $T(i,0)$ at time $t = 0$. Thus, keeping the two "outside" points we can rewrite equation 1.10 in a matrix form where N equation for the "inside" points $i \in [1, N]$ are written in terms of N "inside" and 2 "outside" values of $T(i,j)$. Particularly,

$$\begin{vmatrix} T(1,j+1) \\ T(2,j+1) \\ T(3,j+1) \\ \cdots \\ T(N-2,j+1) \\ T(N-1,j+1) \\ T(N,j+1) \end{vmatrix} = \begin{vmatrix} T(1,j) \\ T(2,j) \\ T(3,j) \\ \cdots \\ T(N-2,j) \\ T(N-1,j) \\ T(N,j) \end{vmatrix} + \frac{dt}{dx^2}(T(0,j)) \begin{vmatrix} 1 \\ 0 \\ 0 \\ \cdots \\ 0 \\ 0 \\ 0 \end{vmatrix} + \begin{pmatrix} -2 & 1 & & & & & \\ 1 & -2 & 1 & & & & \\ & 1 & -2 & 1 & & & \\ & & \cdot & \cdot & \cdot & & \\ & & & 1 & -2 & 1 & \\ & & & & 1 & -2 & 1 \\ & & & & & 1 & -2 \end{pmatrix} \begin{vmatrix} T(1,j) \\ T(2,j) \\ T(3,j) \\ \cdots \\ T(N-2,j) \\ T(N-1,j) \\ T(N,j) \end{vmatrix} + T(N+1,j) \begin{vmatrix} 0 \\ 0 \\ 0 \\ \cdots \\ 0 \\ 0 \\ 1 \end{vmatrix}). \tag{1.11}$$

One of the boundary conditions $T(N,j) = T_0$, $j \geq 0$ can be implemented by noticing that solution of equation 1.11 satisfy this condition only if $T(N,j+1) =$

$T(N,j)$ for all $j \geq 0$. This leads to $T(N-1,j) - 2T(N,j) + T(N+1,j) = 0$ for all $j \geq 0$. This last equations means that

$$T(N+1,j) = 2T_0 - T(N-1,j) \tag{1.12}$$

for all $j \geq 0$.

As far as the second boundary condition $\frac{\partial T(x,t)}{\partial x}|_{x=0} = -\eta(T_R - T(0,t))$ is concerned, we first rewrite it in a discretized form $\frac{\partial T(i,j)}{\partial i}|_{i=1} = -\eta(T_R - T(1,j))$ and then approximate a discretized first order derivative by the methods described above. As the discretized second order derivative is approximated to the $O(dx^2)$ one has to approximate the first order discretized spatial derivative to the $O(dx^3)$ to achieve an overall accuracy of the finite difference scheme of $O(dx^2)$. One such representation of $\frac{\partial T(i,j)}{\partial i}|_{i=1}$ can be chosen as

$$\frac{\partial T(i,j)}{\partial i}|_{i=1} = \frac{-\frac{1}{6}T(3,j) + T(2,j) - \frac{1}{2}T(1,j) - \frac{1}{3}T(0,j)}{dx} + O(dx^3). \tag{1.13}$$

Consequently, to the $O(dx^3)$ the second boundary condition can be written as

$$\frac{-\frac{1}{6}T(3,j) + T(2,j) - \frac{1}{2}T(1,j) - \frac{1}{3}T(0,j)}{dx} = -\eta(T_R - T(1,j)). \tag{1.14}$$

From the last equation $T(0,j)$ can be expressed via $T(1,j), T(2,j), T(3,j)$ as

$$T(0,j) = -\frac{1}{2}T(3,j) + 3T(2,j) - (\frac{3}{2} + 3dx\eta)T(1,j) + 3dx\eta T_R \tag{1.15}$$

for all $j \geq 0$.

Finally, substitution of the values 1.12, 1.15 at the "outside" points $T(0,j), T(N+1,j)$ as defined by the discretized boundary conditions into equation 1.11 leads to the following matrix equations for the heat flow problem in a slender rod subjected to the boundary conditions 1.2, 1.3

$$\begin{vmatrix} T(1,j+1) \\ T(2,j+1) \\ T(3,j+1) \\ \cdots \\ T(N-2,j+1) \\ T(N-1,j+1) \\ T(N,j+1) \end{vmatrix} = \begin{vmatrix} T(1,j) \\ T(2,j) \\ T(3,j) \\ \cdots \\ T(N-2,j) \\ T(N-1,j) \\ T(N,j) \end{vmatrix} + \begin{vmatrix} T_{xx}(1,j) \\ T_{xx}(2,j) \\ T_{xx}(3,j) \\ \cdots \\ T_{xx}(N-2,j) \\ T_{xx}(N-1,j) \\ T_{xx}(N,j) \end{vmatrix}, \tag{1.16}$$

where a discretized second order spatial operator satisfying required boundary conditions is given as

$$\begin{vmatrix} T_{xx}(1,j) \\ T_{xx}(2,j) \\ T_{xx}(3,j) \\ \cdots \\ T_{xx}(N-2,j) \\ T_{xx}(N-1,j) \\ T_{xx}(N,j) \end{vmatrix} = \frac{dt}{dx^2}\left(\begin{pmatrix} -\frac{7}{2}-3dx\eta & 4 & -\frac{1}{2} & & & & & \\ 1 & -2 & 1 & & & & & \\ & 1 & -2 & 1 & & & & \\ & & \cdot & \cdot & \cdot & & & \\ & & & 1 & -2 & 1 & & \\ & & & & 1 & -2 & 1 & \\ & & & & & 0 & -2 & \end{pmatrix} \begin{vmatrix} T(1,j) \\ T(2,j) \\ T(3,j) \\ \cdots \\ T(N-2,j) \\ T(N-1,j) \\ T(N,j) \end{vmatrix} + \begin{vmatrix} 3dx\eta T_R \\ 0 \\ 0 \\ \cdots \\ 0 \\ 0 \\ 2T_0 \end{vmatrix} \right). \tag{1.17}$$

Starting from an initial temperature distribution in the rod $T(idx,t)|_{t=0}$ one has to iterate relation 1.17 to find a discretized temperature profile $T(i,j)$ at the following time moments jdt.

1.1.3 Stability analysis

As we have seen in the previous section there are many ways of defining a particular approximations to the true finite difference operators. Thus, some criterion is necessary that would help us to decide whether a particular form of an approximation to the finite different operators would result in overall stable or unstable iteration scheme. For a wide variety of PDE's such a criterion does exist and is known as von Neumann stability analysis method. In the case of the heat transfer equation the normal modes of equation 1.5 have the form (I is defined to be a unitary pure complex)

$$T_k(x,t) \sim exp(Ikx - \lambda(k)t) \tag{1.18}$$

where, normally, $\lambda(k) > 0$ and real for any extended mode with a real value of k. Normal modes with real $\lambda(k) > 0$ correspond to the stable solutions that are finite with time. However, if an approximation to the finite difference operators is not chosen carefully it can allow for the real k's for which the normal modes possess

$Re(\lambda(k)) < 0$. These modes correspond to the unstable solutions that grow in time. Due to the numerical noise these unstable modes of equation 1.5 will be inevitably excited during iterations thus making an overall scheme unstable.

To demonstrate this point consider a finite difference approximation to the heat transfer equations 1.10 used in the previous section

$$\frac{T(i+1,j) - 2T(i,j) + T(i-1,j)}{dx^2} = \frac{T(i,j+1) - T(i,j)}{dt}. \tag{1.19}$$

Let us look for the normal modes in a form (1.18)

$$T_k(i,j) \sim exp(Ikidx - \lambda(k)jdt). \tag{1.20}$$

Substitution of the above normal modes into (1.10) leads to the following relation between $\lambda(k)$ and k

$$\lambda(k) = \frac{1}{dt} log(\frac{1}{1 - \frac{4dt}{dx^2} sin^2(\frac{kdx}{2})}). \tag{1.21}$$

A simple analysis of the above equation shows that in order for the $\lambda(k)$ to be real and greater than zero for all real k it is necessary that $\frac{4dt}{dx^2} < 1$.

Thus, for a discretized approximation 1.10 of the heat flow equations 1.4 to provide a stable iteration scheme the time step dt has to be chosen to be less then $\frac{dx^2}{2}$.

1.1.4 Implementation of linear constraints

Consider now a slightly more complicated experimental setup in which one end of the rod is submerged into a thermostat at T_0 as previously, while the other end instead of been sticking out into the air, is placed into another thermostat which temperature can be controlled at will by an operator (see figure 1-2).

Suppose now that we would like to control an average temperature over the rod to be some specific function of time $\bar{T}(t)$. As an average temperature over the rod is defined as $\bar{T}(t) = \int T(x,t)dx$, in discretized form it can be expressed as $\bar{T}(jdt) \simeq \frac{1}{N-1} \sum_{i=1}^{N} T(i,j)$ which is a linear function of the temperature values at different spatial points. The linear constraint $\bar{T}(jdt) \simeq \frac{1}{N-1} \sum_{i=1}^{N} T(i,j)$ can be easily

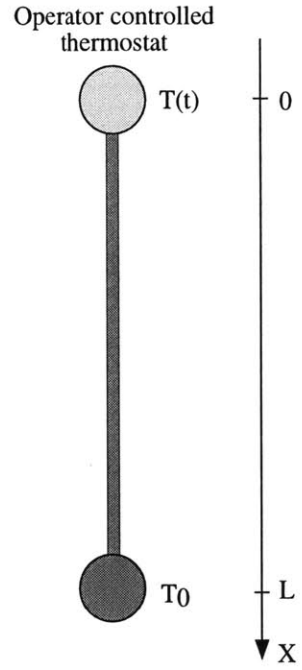

Figure 1-2: Model of an experimental setup where the temperature at the upper end can be controlled by the operator. Given such freedom one can manually control a heat flow into a system.

implemented in the framework of the finite difference scheme described above. Experimentally, to impose such a constraint an operator has to vary the temperature of the thermostat at the upper end of the rod in some specific fashion. To formulate this we now want to model how the temperature of the upper thermostat should be varied so that the average temperature of the rod follows a predesigned time dependence $\bar{T}(t)$.

Equations and boundary conditions governing the heat flow in the problem can be written as

$$\begin{cases} \frac{\partial^2 T(x,t)}{\partial x^2} &= \frac{\partial T(x,t)}{\partial t}, \\ T(x,t)|_{x=1} &= T_0, \\ \int_0^1 T(x,t) &= \bar{T}(t). \end{cases} \tag{1.22}$$

As before, we incorporate one of the boundary conditions into the form of a discretized second order spatial operator using an "outside" variable $T(N+1,j)$ which leaves the other "outside" variable $T(0,j)$ undefined. A discretized version of the above

equations to the $O(dx^2)$ and $O(dt)$ can be written as

$$\begin{vmatrix} T(1,j+1) \\ T(2,j+1) \\ T(3,j+1) \\ \cdots \\ T(N-2,j+1) \\ T(N-1,j+1) \\ T(N,j+1) \end{vmatrix} = \begin{vmatrix} T(1,j) \\ T(2,j) \\ T(3,j) \\ \cdots \\ T(N-2,j) \\ T(N-1,j) \\ T(N,j) \end{vmatrix} + \frac{dt}{dx^2}(T(0,j)) \begin{vmatrix} 1 \\ 0 \\ 0 \\ \cdots \\ 0 \\ 0 \\ 0 \end{vmatrix} + \begin{pmatrix} -2 & 1 & & & & & \\ 1 & -2 & 1 & & & & \\ & 1 & -2 & 1 & & & \\ & & \cdot & \cdot & \cdot & & \\ & & & 1 & -2 & 1 & \\ & & & & 1 & -2 & 1 \\ & & & & & 0 & -2 \end{pmatrix} \begin{vmatrix} T(1,j) \\ T(2,j) \\ T(3,j) \\ \cdots \\ T(N-2,j) \\ T(N-1,j) \\ T(N,j) \end{vmatrix} + \begin{vmatrix} 0 \\ 0 \\ 0 \\ \cdots \\ 0 \\ 0 \\ 2T_0 \end{vmatrix}). \tag{1.23}$$

The constraint condition on average temperature at $t = (j+1)dt$ to the $O(dx^2)$ and $O(dt)$ can be written as

$$\frac{1}{2}T(1,j+1) + \sum_{i=2}^{N-1} T(i,j+1) + \frac{1}{2}T(N,j+1) = (N-1)\bar{T}(j+1). \tag{1.24}$$

Equations 1.23, 1.24 constitute an overall $N+1$ equations with $N+1$ unknowns $\{T(0,j), T(1,j+1), \cdots, T(N,j+1)\}$. Combining equations 1.23, 1.24 gives

$$\begin{pmatrix} 0 & \frac{1}{2} & 1 & 1 & \cdot & 1 & 1 & \frac{1}{2} \\ -\frac{dt}{dx^2} & 1 & 0 & & \cdot & & & \\ & & 1 & & \cdot & & & \\ & & & 1 & \cdot & & & \\ & & & \cdot & \cdot & \cdot & & \\ & & & & \cdot & 1 & & \\ & & & & \cdot & & 1 & \\ & & & & \cdot & & & 1 \end{pmatrix} \begin{vmatrix} T(0,j) \\ T(1,j+1) \\ T(2,j+1) \\ T(3,j+1) \\ \cdots \\ T(N-2,j+1) \\ T(N-1,j+1) \\ T(N,j+1) \end{vmatrix} = \begin{vmatrix} \frac{\bar{T}(j+1)}{dx} \\ 0 \\ 0 \\ 0 \\ \cdots \\ 0 \\ 0 \\ 0 \end{vmatrix} + \begin{vmatrix} 0 \\ T(1,j) \\ T(2,j) \\ T(3,j) \\ \cdots \\ T(N-2,j) \\ T(N-1,j) \\ T(N,j) \end{vmatrix} + \begin{vmatrix} 0 \\ T_{xx}(1,j) \\ T_{xx}(2,j) \\ T_{xx}(3,j) \\ \cdots \\ T_{xx}(N-2,j) \\ T_{xx}(N-1,j) \\ T_{xx}(N,j) \end{vmatrix}, \tag{1.25}$$

where a modified second order operator T_{xx} is defined as

$$\begin{vmatrix} 0 \\ T_{xx}(1,j) \\ T_{xx}(2,j) \\ T_{xx}(3,j) \\ \cdots \\ T_{xx}(N-2,j) \\ T_{xx}(N-1,j) \\ T_{xx}(N,j) \end{vmatrix} = \frac{dt}{dx^2}(\begin{pmatrix} 0 & & & & & & & \\ & -2 & 1 & & & & & \\ & 1 & -2 & 1 & & & & \\ & & 1 & -2 & 1 & & & \\ & & & \cdot & \cdot & \cdot & & \\ & & & & 1 & -2 & 1 & \\ & & & & & 1 & -2 & 1 \\ & & & & & & 0 & -2 \end{pmatrix} \begin{vmatrix} 0 \\ T(1,j) \\ T(2,j) \\ T(3,j) \\ \cdots \\ T(N-2,j) \\ T(N-1,j) \\ T(N,j) \end{vmatrix} + \begin{vmatrix} 0 \\ 0 \\ 0 \\ 0 \\ \cdots \\ 0 \\ 0 \\ 2T_0 \end{vmatrix}). \tag{1.26}$$

Consequently, given a temperature profile at time jdt one can iterate equation 1.25 to find a temperature profile at $(j+1)dt$ that would automatically satisfy required boundary conditions and constraints. Knowing a solution of equation 1.25, time evolution of the temperature of the operator controlled thermostat is given by $T(1,j)$.

1.1.5 Implementation of the non-linear constraints

In a previous section we saw that the linear constraints can be readily implemented by including an extra linear equation into the matrix formulation of a finite difference method. We now address the question of imposing a constraint of a general form such that at any moment of time t the temperature profile $T(x,t)$ is constrained to satisfy $Cr(T(x,t)) = 0$ for some arbitrary functional $Cr(\cdot)$. To tackle this problem we first describe a more general approach for solving a system of algebraic non-linear equations.

Consider a general nonlinear algebraic equation of the form

$$\vec{F}(T_i) = 0 \tag{1.27}$$

where $i \in [0, N]$ and $\vec{F}$ is an $N+1$ dimensional function vector of variables T_i. In general, there are no exact methods of finding a solution of such an equation. In the following, we present an iterative method of solving equation 1.27 also known as nonlinear Newton method. Let T_i^e, $i \in [0, N]$ be an exact solution of equation 1.27. Consider any T_i close to T_i^e. Using a multidimensional Taylor series expansion around T_i^e we can evaluate a value of $\vec{F}(T_i)$ as following

$$\vec{F}(T_i^e) = \vec{F}((T_i^e - T_i) + T_i) = 0, \tag{1.28}$$

and turning to a matrix notation

$$\begin{vmatrix} F_0(T_i) \\ F_1(T_i) \\ \cdot \\ F_{N-1}(T_i) \\ F_N(T_i) \end{vmatrix} + \begin{pmatrix} \frac{\partial F_0(T_i)}{\partial T_0} & \frac{\partial F_0(T_i)}{\partial T_1} & \cdot & \frac{\partial F_0(T_i)}{\partial T_{N-1}} & \frac{\partial F_0(T_i)}{\partial T_N} \\ \frac{\partial F_1(T_i)}{\partial T_0} & \frac{\partial F_1(T_i)}{\partial T_1} & \cdot & \frac{\partial F_1(T_i)}{\partial T_{N-1}} & \frac{\partial F_1(T_i)}{\partial T_N} \\ \cdot & \cdot & \cdot & \cdot & \cdot \\ \frac{\partial F_{N-1}(T_i)}{\partial T_0} & \frac{\partial F_{N-1}(T_i)}{\partial T_1} & \cdot & \frac{\partial F_{N-1}(T_i)}{\partial T_{N-1}} & \frac{\partial F_{N-1}(T_i)}{\partial T_N} \\ \frac{\partial F_N(T_i)}{\partial T_0} & \frac{\partial F_N(T_i)}{\partial T_1} & \cdot & \frac{\partial F_N(T_i)}{\partial T_{N-1}} & \frac{\partial F_N(T_i)}{\partial T_N} \end{pmatrix} \begin{vmatrix} T_0^e - T_0 \\ T_1^e - T_1 \\ \cdot \\ T_{N-1}^e - T_{N-1} \\ T_N^e - T_N \end{vmatrix} + O((T_i^e - T_i)^2) = 0. \tag{1.29}$$

Thus, starting with some approximation T_i to the exact solution T_i^e we can use relation 1.29 to find a supposedly better estimate T_i^b to T_i^e by disregarding $O((T_i^e - T_i)^2)$ and rewriting relation 1.29 as

$$\begin{vmatrix} T_0^b \\ T_1^b \\ . \\ T_{N-1}^b \\ T_N^b \end{vmatrix} = \begin{vmatrix} T_0 \\ T_1 \\ . \\ T_{N-1} \\ T_N \end{vmatrix} - \begin{pmatrix} \frac{\partial F_0(T_i)}{\partial T_0} & \frac{\partial F_0(T_i)}{\partial T_1} & . & \frac{\partial F_0(T_i)}{\partial T_{N-1}} & \frac{\partial F_0(T_i)}{\partial T_N} \\ \frac{\partial F_1(T_i)}{\partial T_0} & \frac{\partial F_1(T_i)}{\partial T_1} & . & \frac{\partial F_1(T_i)}{\partial T_{N-1}} & \frac{\partial F_1(T_i)}{\partial T_N} \\ . & . & . & . & . \\ \frac{\partial F_{N-1}(T_i)}{\partial T_0} & \frac{\partial F_{N-1}(T_i)}{\partial T_1} & . & \frac{\partial F_{N-1}(T_i)}{\partial T_{N-1}} & \frac{\partial F_{N-1}(T_i)}{\partial T_N} \\ \frac{\partial F_N(T_i)}{\partial T_0} & \frac{\partial F_N(T_i)}{\partial T_1} & . & \frac{\partial F_N(T_i)}{\partial T_{N-1}} & \frac{\partial F_N(T_i)}{\partial T_N} \end{pmatrix}^{-1} \begin{vmatrix} F_0(T_i) \\ F_1(T_i) \\ . \\ F_{N-1}(T_i) \\ F_N(T_i) \end{vmatrix} . \quad (1.30)$$

Now using a better approximation T_i^b to the exact solution from relation 1.30 we substitute it back into the same relation 1.30 instead of the old T_i. Implementing such substitutions again and again a self-consistent loop is formed, which in most cases systematically moves T_i^b closer and closer to the exact solution T_i^e. Self-consistent loop can be terminated when $norm(\vec{F}(T_i))$ becomes smaller than a certain error value.

Now we go back to the original problem of imposing the nonlinear constraints in a framework of the finite difference scheme of solving PDE's. As shown in the previous section, finite difference representation of the heat flow equations in matrix notation takes the following general form

$$AT(i, j+1) + BT(i, j) + C = 0 \quad (1.31)$$

where $i \in [0, ..., N]$, A and B are the $(N \times (N+1))$ matrices and C is an N dimensional vector. Thus, finite difference operators involve $N+1$ unknowns $T(i, j+1)$,$i \in [0, ..., N]$ and N equations. An extra equation required to find a solution to equation 1.31 is given by a discretized constraint $Cr(T(i, j+1)) = 0$.

Next, we construct an $N+1$ dimensional vector $\vec{F}(T(i, j))$ of the following form

$$\begin{vmatrix} F_0(T(i, j+1)) \\ F_{1..N}(T(i, j+1)) \end{vmatrix} = \begin{pmatrix} Cr(T(i, j+1)) \\ AT(0..N, j+1) + BT(0..N, j) + C \end{pmatrix} . \quad (1.32)$$

The problem of solving equation 1.31 with a constraint $Cr(T(x, t)) = 0$ can now be reformulated in terms of solving a nonlinear algebraic equation $\vec{F}(T(i, j)) = 0$ with a functional vector $\vec{F}(T(i, j))$ defined by relation 1.32. Using a nonlinear Newton method described above for solving such a multidimensional nonlinear set of equations one can find a solution which would automatically satisfy all the necessary boundary

conditions and nonlinear constraints.

We would like to conclude this section by summarizing that final difference methods are based on the intuitive idea of representing the continuous functions and their operators in a discretized form. These methods are especially convenient in the finite domain where the spatial dimensions are bounded so that the problem of having an infinite number of discretization points to represent functions on such a domain wouldn't arise. The finite difference methods gained a wide popularity because of a clear intuition behind them and they are used in many practical applications.

1.2 Solution of PDE's using an expansion of a trial solution into a functional basis set.

In this section we are going to discuss a different class of PDE's describing wave propagation phenomenon. A large set of problems in engineering and physics involves wave propagation in some media. These waves can have electro-magnetic, mechanical or even quantum nature. Functions that describe waves are typically extended over an entire infinite spatial domain and simulation of such waves in a framework of the finite difference methods becomes computationally inconvenient. Another, more important reason for finite difference methods to become inefficient in dealing with waves is in the wave's inherent time dependent oscillatory nature. Ordinary, waves are characterized by their periodicity in a spatial domain determined by the wavelength λ, and their temporal periodicity determined by the frequency ω of wave oscillations in time. If one were to simulate the behavior of the waves over the time of many periods finite difference methods may become very computationally inefficient. Particularly, as we have seen before, the condition of stability of a finite difference method frequently imposes a limitation on a discretization time step. If a period of the wave under study is much greater than an allowed discretization time step sampling over many time periods can become very computationally time consuming.

To circumvent these problems one can try the following approach. Suppose

$\phi_{k,\omega}(x,t)$, is a set of functions possessing wave-like properties and each characterized by numbers k and ω. By that we mean that for each k, ω function $\phi_{k,\omega}(x,t)$ is defined over an infinite spatial domain and it is periodic in space and time. In calculus it is proved that under some general conditions any well-behaved function $E(x,t)$ can be expanded in terms of a complete set of $\phi_{k,\omega}(x,t)$ so that

$$E(x,t) = \int dk \int d\omega C_{k,\omega}\phi_{k,\omega}(x,t). \tag{1.33}$$

A collection of such $\phi_{k,\omega}(x,t)$ is called a basis set. As an example, a frequently used basis set particularly useful to simulate infinite periodic systems is a planewave basis set where the basis functions are as following

$$\phi_{k,\omega}(x,t) = \frac{1}{2\pi} exp(ixk - i\omega t). \tag{1.34}$$

Thus, for a particular wave equation finding a solution is equivalent to finding an infinite set of basis coefficients $C_{k,\omega}$ in equation 1.33 where ω is commonly a function of k. An apparent advantage of using a basis set in a form of relation 1.33 is that a multi-dimensional (in this case variables x and t) oscillatory problem is frequently reduced to a lover dimensional problem of finding $C_{k,\omega(k)}$ in "k" space. Another advantage is that $C_{k,\omega(k)}$ is usually not zero only on some finite number of spatially confined intervals. Finally, one doesn't have to approximate the derivatives of the PDE's as soon the basis function used are sufficiently well behaved. In spite of all the advantages of this method for finding an oscillatory waveforms one have to be careful to include a sufficiently large number of the basis functions to achieve any meaningful solution. Also, for some problems, one has to use very special basis sets if a truthful description of sharp spatial variations of the waveforms is necessary [3].

In the following, we consider an application of the method using a planewave expansion of a trial solution to a problem of finding a form of the electro-magnetic states in a media characterized by a periodic dielectric constant (a so called photonic crystal). On figure 1-3, a one dimensional photonic crystal is sketched.

There, R is a periodicity of a photonic crystal and R_1, R_2 are the widths of the

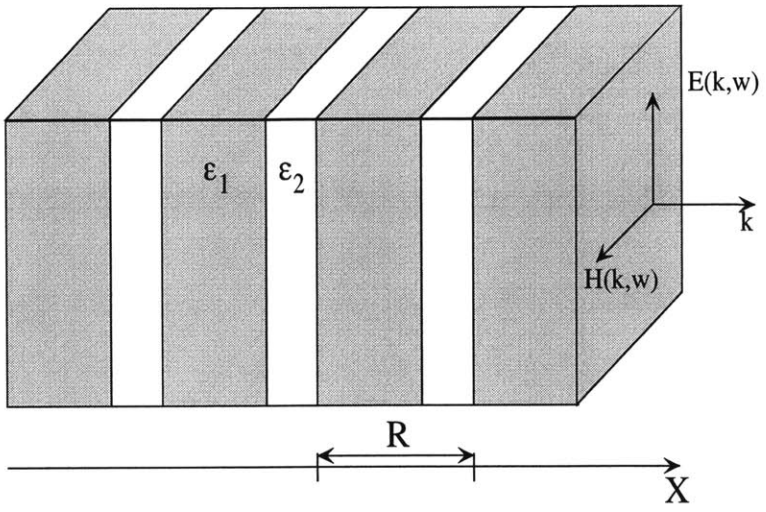

Figure 1-3: A sketch of a one dimensional photonic crystal made of the periodically repeated slabs of two different dielectrics. Here, R is the periodicity of a photonic crystal and R_1, R_2 are the widths of the slabs with dielectric constants ϵ_1 and ϵ_2 respectively. Also shown the directions of the electric and magnetic fields as well as a direction of a wave propagation for the photonic crystal modes studied in this section.

slabs with dielectric constants ϵ_1 and ϵ_2 respectively. We start analyzing this system by writing Maxwell's equations for the electro-magnetic fields in a non magnetic material with a position dependent periodic dielectric constant $\epsilon(x+R) = \epsilon(x)$

$$\begin{cases} \bigtriangledown \times H(x,t) &= \frac{\partial(\epsilon(x)E(x,t))}{\partial ct} \\ \bigtriangledown \times E(x,t) &= -\frac{\partial H(x,t)}{\partial ct} \end{cases} \tag{1.35}$$

where $E(x,t)$ and $H(x,t)$ are the electric and magnetic fields at the moment of time t. Because of the spatial periodicity of a dielectric constant it can be decomposed in terms of a countable set of planewave basis functions as

$$\epsilon(x) = \sum_G \epsilon_G \exp(iGx) \tag{1.36}$$

where reciprocal vectors G are defined as $G = n\frac{2\pi}{R}$, $n \in \{-\infty, ..., -1, 0, 1, ..., +\infty\}$. It is known from a theory of photonic crystals (Bloch theorem) that electro-magnetic

modes in such a system can be characterized by a wavevector q and a countable set of band frequencies $\{\omega_1(q), \omega_2(q), ...\}$. A general form of a solution of equation 1.35 in a planewave basis set can be written as following

$$\begin{vmatrix} H_{q,\omega(q)}(x,t) \\ E_{q,\omega(q)}(x,t) \end{vmatrix} = exp(iqx - i\omega(q)t) \sum_G \begin{vmatrix} H_G(q) \\ E_G(q) \end{vmatrix} exp(iGx) \qquad (1.37)$$

where $\begin{vmatrix} H_G(q) \\ E_G(q) \end{vmatrix}$ are the expansion coefficients of the electro-magnetic modes in a planewave basis set. Substituting relations 1.37, 1.36 into equation 1.35 and using the orthogonality of the planewave basis functions one can rewrite equation 1.35 in terms of the expansion coefficients $\begin{vmatrix} H_G(q) \\ E_G(q) \end{vmatrix}$ as

$$\begin{cases} (G+q)H_G(q) &= -\frac{\omega}{c} \sum_G \epsilon_{(G'-G)} E_G(q) \\ (G+q)E_G(q) &= -\frac{\omega}{c} H_G(q) \end{cases} . \qquad (1.38)$$

Finally, substitution of the equations (1.38) into each other gives

$$\left\{ (G+q)^2 E_G(q) = \frac{\omega^2}{c^2} \sum_G \epsilon_{(G'-G)} E_G(q) \right. . \qquad (1.39)$$

Rewriting the above equation in a matrix form and redefining $G = \frac{2\pi}{R}$ we rewrite equation 1.39 in a matrix form as

$$\begin{pmatrix} \cdot & & & & & \\ & (q+2G)^2 & & & & \\ & & (q+G)^2 & & & \\ & & & q^2 & & \\ & & & & (q-G)^2 & \\ & & & & & (q-2G)^2 \\ & & & & & \cdot \end{pmatrix} \begin{vmatrix} \cdot \\ E_{2G}(q) \\ E_G(q) \\ E_0(q) \\ E_{-G}(q) \\ E_{-2G}(q) \\ \cdot \end{vmatrix} = \frac{\omega^2}{c^2} \begin{pmatrix} \cdot & \cdot & \cdot & \cdot & \cdot & \cdot & \cdot \\ \cdot & \epsilon_0 & \epsilon_G & \epsilon_{2G} & \epsilon_{3G} & \epsilon_{4G} & \cdot \\ \cdot & \epsilon_{-G} & \epsilon_0 & \epsilon_G & \epsilon_{2G} & \epsilon_{3G} & \cdot \\ \cdot & \epsilon_{-2G} & \epsilon_{-G} & \epsilon_0 & \epsilon_G & \epsilon_{2G} & \cdot \\ \cdot & \epsilon_{-3G} & \epsilon_{-2G} & \epsilon_{-G} & \epsilon_0 & \epsilon_G & \cdot \\ \cdot & \epsilon_{-4G} & \epsilon_{-3G} & \epsilon_{-2G} & \epsilon_{-G} & \epsilon_0 & \cdot \\ \cdot & \cdot & \cdot & \cdot & \cdot & \cdot & \cdot \end{pmatrix} \begin{vmatrix} \cdot \\ E_{2G}(q) \\ E_G(q) \\ E_0(q) \\ E_{-G}(q) \\ E_{-2G}(q) \\ \cdot \end{vmatrix} . \qquad (1.40)$$

Equation 1.40 represent an eigen value problem where ω^2 is an eigen value and a set of the expansion coefficients $\{E_{nG}\}$ corresponds to an eigen-vector. Solving for these quantities and substituting them back into relation 1.37 gives a solution for the electro-magnetic fields in a system with a periodic dielectric constant.

In general, using the methods with a functional basis transforms the problem of solving a system of the multidimensional PDE's to a (supposedly simpler) problem of finding a solution (in terms of the expansion coefficients) of some highly dimensional nonlinear algebraic equation. For some PDE's (particularly, for a wave-type PDE's) using such methods frequently transforms the problem into an eigen value problem which can be readily solved by standard methods, while for a general PDE a transformed problem can be as complex as an original one.

In the following, we apply the methods described in this chapter to the research problems the author was involved in at the Department of Physics (under the guidance of Prof. J.D. Joannopoulos) and the Department of Mechanical Engineering (under the guidance of Prof. L. Mahadevan) at MIT.

Chapter 2

Folding of Viscous Sheets and Filaments

We consider the nonlinear folding behavior of a viscous filament or a sheet under the influence of an external force such as gravity. An example is provided by pouring a sheet of honey onto a table from a sufficient height. Near the table, the sheet forms a series of periodic folds much as an elastic sheet fed towards a horizontal surface would. Another example is a folding of a soap filament confined to a soap film stretched on a frame (this was discovered by the author while refilling a soup bottle). When the filament reaches the bottom of the frame it forms a series of folds. Using an analogy to the elastic case, we derive a set of equations for the planar dynamics of viscous sheets and filaments, and solve them numerically to follow the evolution of a fold under the influence of gravity. We also give scaling laws for the size of the folds and the frequency with which they are laid out.

The buckling of solids is a well established subject whose origins date back to the work of L. Euler and Joh. Bernoulli. This instability which arises as a result of the competition between axial compression and bending in slender objects is not restricted to solids; it can also occur in creeping flows of fluids in slender geometries [4]. As in the case of solids, the buckling, folding, and coiling of thin sheets and filaments of fluids occurs on length scales spanning several orders of magnitude, from geophysics [5] figure 2-1 a) to soft-matter physics [6] figures 2-1 b),c). A simple demonstration

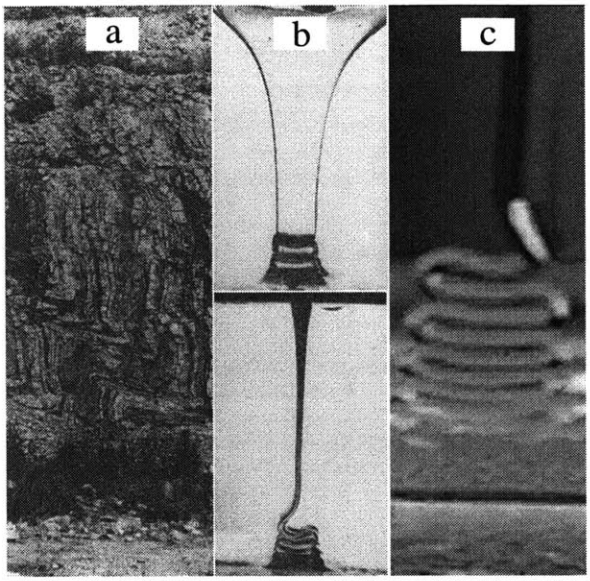

Figure 2-1: Photographs of some instances of viscous folding. (a) folds in rock formations have typical wavelengths of the order of a few m. (b) A viscous sheet of honey falling vertically on a substrate forms a set of periodic folds with a typical wavelength of a few cm. (c) A viscous soap filament falling vertically in a thin soap film folds periodically with a wavelength of the order of a few mm.

of this latter instability is a daily occurrence at the breakfast table. When honey is poured onto toast from a sufficient height, near the surface the thin filament whirls steadily about the vertical laying out a regular helical coil [7]. A two-dimensional analog of this process, viz. the folding of a viscous sheet is also easy to observe when a sheet of honey is poured onto a surface.

In fact, the flow patterns that one observes on the horizontal surface are directly correlated with the cross-section of the impinging liquid; viscous fluids flowing from a small height always spread out axisymmetrically, round filaments form coils, while sheets fold. In the last case, as the height of fall is increased, the edges of the sheet come together under the influence of surface tension changing the sheet width, until it eventually becomes an axisymmetric filament that in turn coils. To observe folding patterns over a range of falling heights we must confine the flow to two dimensions. This can be achieved in a number of ways, such as pinning the lateral edges of a flowing viscous sheet using threads, using a vertical Hele-Shaw cell, or by using a thin

viscous soap film flowing vertically, and then allowing a large drop of soap to fall in it (see figure 2-1 c)). As the drop falls, it is stretched out under the influence of gravity while speeding up. When the filament reaches the bottom of the frame, it forms a series of folds, exactly like a thin sheet of paper that is fed towards the floor [8]. In this letter we will consider the folding of a filament confined to lie in the plane, as in a soap film, and later discuss variants of this phenomenon.

2.1 Formation of a fold

The physical parameters governing the phenomena include the fluid viscosity μ (kinematic viscosity $\nu = \mu/\rho$), the flow rate Q, gravity g, a characteristic filament radius r and the height h over which the filament falls. As h is gradually increased, the axial stagnation flow becomes unstable to bending disturbances and the filament is laid out in a series of periodic folds of length L at a frequency Ω. The onset of the instability [9] is determined by the relative magnitude of a gravitational time scale $(h/g)^{1/2}$ and a viscous time scale $r^2\rho/\mu$ characterized by a Reynolds number $Re = gr^3/\nu^2$. A similar parameter $\rho g h^3/B$, where B is the bending stiffness occurs in the elastic analogue [8]. Only below a critical value of the aspect ratio of the filament r/h or Re is the axisymmetric stagnation flow unstable. When aspect ratio becomes sufficiently small (but still is far from the onset), the flow is still mainly an axial stretching flow corresponding to the "outer" region. However in a small neighborhood of the flat surface that constitutes a "bending boundary layer", there is a highly nonlinear folding region, as seen in figure 2-1 b),c).

For low folding frequencies, the filament inertia is unimportant when $\Omega \ll (\frac{L}{g})^{\frac{1}{2}}$. We will assume that this inequality is valid: then the dynamics of folding are determined by the balance between the forces due to gravity and viscosity. Observations of a filament that is fed from far above a horizontal plane reveal various stages in the folding process, as shown in figure 2-2.

Close to the bottom of the frame where the folding occurs, the filament diameter is essentially unchanged, although its center line is highly curved. During the formation

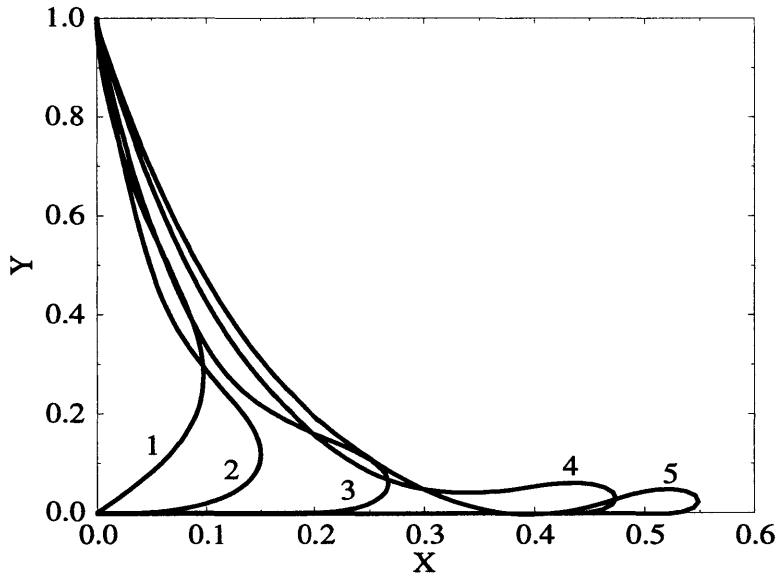

Figure 2-2: 1) Beginning of folding, filament touches the bottom and buckles on contact. 2) Further flow causes the filament to become tangential to the horizontal surface at the point of contact. 3) Contact point starts moving from the origin. 4) Further flow causes the central line to move downwards. 5) Moving of the central line downwards proceeds until the central line touches itself.

of a single fold, the filament buckles on contact; further flow causes the filament to become tangential to the horizontal surface at the point of contact. Still further flow causes the contact point to move, as an incipient fold is laid out. This continues until the point of inflection in the center line begins to move downwards instead of outwards; eventually the filament touches itself forming a second contact point. The filament rolls briefly about this new contact point until the curvature at this contact point vanishes; then a third contact point is born at this location and moves until it is directly below the feeding point,leading to the formation of a half-fold. An identical scenario on the opposite side leads to the formation of the second half of the periodic fold. The next fold is laid out on the previous one; if the height from which the filament is fed is large compared to the height of the fold we only need to consider the formation of a single fold owing to the periodicity of the phenomenon.

2.2 Scaling laws

To investigate the role of the various physical parameters in the problem, we start with dimensional analysis. The six parameters of importance in this problem are the viscosity of a fluid μ, the density of a fluid ρ, the moment of inertia $I = \frac{\pi r^4}{2}$ of the crossection of the filament where r is a radius of a filament, the height h from which the filament is fed, the feeding velocity v and the acceleration of gravity g. As their dimensions are expressible in terms of mass, length and time, according to the Buckingham Pi theorem, the number of independent dimensionless parameters is three, say

$$\begin{aligned} \eta &= \frac{\mu r^2 v}{\rho g h^4} \\ \gamma &= \frac{v^2}{gh} \\ \zeta &= \frac{I}{h^4}. \end{aligned} \tag{2.1}$$

Thus the fold period and length, is a function of these three parameters

$$\begin{aligned} T_f &= \frac{h}{v} f(\eta, \gamma, \zeta) \\ L_f &= hg(\eta, \gamma, \zeta). \end{aligned} \tag{2.2}$$

If the filament is fed slowly so that the inertial forces are negligible, then $\gamma \ll 1$. For typical viscous materials $\eta \gg \zeta$ and $\zeta \ll 1$ so that

$$\begin{aligned} T_f &= \frac{h}{v} f(\eta, \gamma, \zeta) \sim \frac{h}{v} t(\eta, 0, 0) \\ L_f &= hg(\eta, \gamma, \zeta) \sim hg(\eta, 0, 0). \end{aligned} \tag{2.3}$$

As the drop height h is increased indefinitely we expect a finite limit for T_f and L_f thus, functions $t(\eta, 0, 0)$ and $g(\eta, 0, 0)$ must be proportional to $\eta^{\frac{1}{4}}$ so that

$$\begin{aligned} T_f &\sim \frac{h}{v} \eta^{\frac{1}{4}} \\ L_f &\sim h\eta^{\frac{1}{4}}. \end{aligned} \tag{2.4}$$

For $\eta << 1$, a simple argument that balances viscous and gravitational forces reveals the nature of this dependence. In the neighborhood of a fold of length L, the filament turns around a bend of radius L at velocity v without a change in its diameter;

therefore the axial viscous stress is linear in the depth and scales as $\mu r v/L^2$. The depth-integrated stress resultant vanishes as a consequence, but the depth integrated torque scales as $\mu r^4 v/L^2$. This is balanced by a gravitational torque of magnitude $\rho g r^2 L^2$. This leads to the following scaling laws for the fold length L and the folding frequency $\Omega \sim v/L$

$$\begin{aligned} L &\sim (\nu v r^2/g)^{1/4} &&\sim \eta^{1/4} h \\ \Omega &\sim (\nu r^2/g v^3)^{-1/4} &&\sim \eta^{-1/4} v/h. \end{aligned} \tag{2.5}$$

2.3 Theoretical formulation

In the region where the filament is being stretched axisymmetrically, a depth-integrated version of the Stokes' equations yields $\mu(r^2 u_z)_z = \rho g r^2$, where $r = r(z,t)$ is the radius of the filament at a vertical location z below the feeding point, and $u(z,t)$ is the axial velocity. This leading order asymptotic equation ignores the effects of inertia and surface tension, assumes that the axial velocity profile is plug-like, and that the effect of the surrounding fluid is negligible. A solution of the axially stretching flow provides the outer solution for the flow velocity v and the filament diameter $2r$ that must be matched to the solution in the folding regime near the bottom boundary. Since the height of this last regime is so small compared to the total fall height, we can neglect it and solve the outer problem over the entire height of fall h in principle.

In the folding regime, the filament is assumed to have a circular cross-section and is confined to two dimensions. Therefore, we can characterize the filament by its center line in terms of the arc-length s and the angle $\phi(s,t)$ between the tangent to the center line and the x axis. Letting $n_1(s,t)$ and $n_2(s,t)$ be the integrated stress resultants in the x and y directions and $m(s,t)$ be the bending moment in the z direction (see figure 2-3), we can write the following equations for the balance of

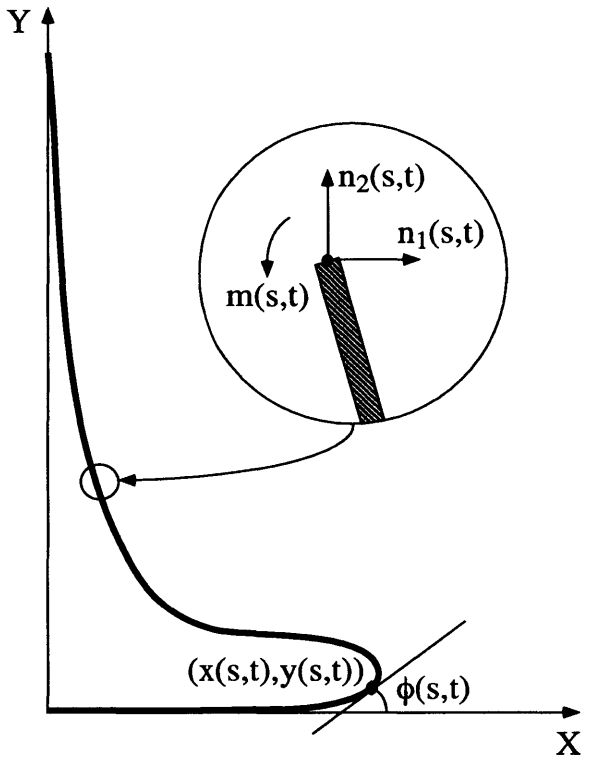

Figure 2-3: A schematic of a viscous filament of constant diameter flowing around a bend under the influence of gravity. If the filament is not being stretched or compressed, its center line can be parameterized in terms of its arc-length s. The filament can then be described by the location of its center line $x(s,t), y(s,t)$, and the orientation of its cross-section, $\phi(s,t)$ being the angle between the tangent to the center line and the horizontal. The components of the depth-integrated stress in the horizontal and vertical directions are $n_1(s,t)$ and $n_2(s,t)$ respectively.

horizontal and vertical forces, and moments

$$\begin{cases} n_{1s} &= 0, \\ n_{2s} &= \rho g, \quad 0 \leq s \leq vt, \\ m_s &= n_1 sin\phi(s) - n_2 cos\phi(s) \end{cases} \tag{2.6}$$

where $(\cdots)_s = \partial(\cdots)/\partial s$, and vt is the total length of the filament being at velocity v.

These equations are 1-dimensional approximations to the 3-dimensional equations of equilibrium and are valid for a slender filament in the long-wavelength limit. For

completeness, they must be supplemented by a fourth equation relating the variables n_1, n_2, m, ϕ. Since the dominant deformation of the filament during folding is due to bending, a natural candidate is a relation between the curvature $\phi_s(s,t)$ and the torque. For a slender elastic filament, the axial strain ϵ due to bending varies linearly with the diameter and inversely with the radius of curvature [10], so that the stress $\sigma = Er\phi_s$. Integrating the stress through the cross-section leads to a vanishing resultant; however the moment $m = \int \sigma r dA$ does not vanish, and yields $m \sim Er^4\phi_s$, For a viscous filament, the stress is proportional to the strain rate, so that the viscous stress $\sigma = \mu(r\phi_s)_t = \mu r\phi_{st}$, if the filament diameter is unchanged, as in our case. Therefore, for a viscous filament, $m \sim \mu r^4\phi_{st}$. This heuristic argument can be formalized as a leading order asymptotic theory derived from Stokes' equation for a slender filament of small aspect ratio, with the center line capable of having large curvatures [11], and leads to

$$m = 3\mu r^4\phi_{st}. \tag{2.7}$$

Equations (1-2) are sufficient to determine ϕ, n_1, n_2; we note that the stress resultants n_1, n_2 are determined by the boundary conditions and in fact are Lagrange multipliers that enforce the constraints of inextensibility and vanishing transverse velocity gradients. Upon defining the dimensionless variables $\bar{s} = \frac{s}{h}, \bar{t} = \frac{tv}{h}, \bar{n}_{1,2} = \frac{n_{1,2}}{\rho g h}$, with h being the height from which the filament is being fed by the axial flow. Then the equations 2.6, 2.7 can be rewritten, on dropping the bars, as

$$\begin{cases} n_{1s} &= 0, \\ n_{2s} &= 1, \quad 0 \le s \le 1+t, \\ \eta\phi_{sst}(s,t) &= n_1 sin\phi(s) - n_2 cos\phi(s) \end{cases} \tag{2.8}$$

where $\eta = 3\mu r^2 v/\rho g h^4$ is a scaled viscous bending resistance, and we start the clock when the filament first touches the bottom plate. In a typical experiment, $\mu \sim 10 Pa.s, r = 10^{-3}m, v = 0.1m/s, \rho = 10^3 kg/m^3, h = 0.1m$ so that $\eta \sim 10^{-6}$. Therefore, we expect the filament to be straight and vertical over most of its length, with the fold limited to a very small region near the floor. Once we have solved

equation 2.8, the shape of the filament at any instant is determined by integrating the two kinematic relations $x_s = \cos\phi, y_s = \sin\phi$. During the evolution of a fold, the boundary conditions must be specified at the unknown contact points, and must be changed at certain critical points. To facilitate the numerical solution of this problem, we keep the domain of the problem fixed to $s \in [0,1]$, rescaling all lengths by defining $\xi = \frac{s}{l_i+(t-t_i)-(s_i(t)-s_i(t_i))}$ where $(\xi \in [0,1])$, $s_i(t)$ is the location of the i^{th} contact point, l_i is the length of the filament between the feeding point and the last contact point at the time t_i when the i^{th} contact point have emerged. Then equations 2.8 transform into

$$\begin{cases} n_{1\xi} &= 0, \\ n_{2\xi} &= (l_i + (t-t_i) - (s_i(t) - s_i(t_i))), \\ \eta\phi_{\xi\xi t}(\xi,t) &= \eta\frac{2(1-s_{it}(t))}{l_i+(t-t_i)-(s_i(t)-s_i(t_i))}\phi(\xi,t)_{\xi\xi} + (n_1 sin\phi(\xi,t) - n_2 cos\phi(\xi,t))(l_i + (t-t_i) - (s_i(t) - s_i(t_i)))^2. \end{cases} \tag{2.9}$$

The boundary conditions at the feeding point are

$$\begin{array}{lllll} \phi(1,t) &= \frac{\pi}{2}, & & & \\ x(1,t) &= \frac{s_i(t)}{l_i+(t-t_i)-(s_i(t)-s_i(t_i))} + \int_0^1 cos\phi(\xi,t)d\xi &= 0, & \\ y(1,t) &= \int_0^1 sin\phi(\xi,t)d\xi & = \frac{1}{l_i+(t-t_i)-(s_i(t)-s_i(t_i))}. & \end{array} \tag{2.10}$$

The first condition is due to the vertical feeding of the filament, while the second and third characterize the location of the feeding point as measured from the latest contact point $s_i(t)$, with $s_0(t) = 0,\ \ l_0 = 1,\ \ t_0 = 0$. The boundary conditions at the contact point which always lies on the same horizontal plane vary. Once the filament has contacted the horizontal surface (at $t = 0$), the filament buckles, and pivots about the point of contact assumed to be at the origin so that

$$\phi_\xi(0,t) = 0, \quad x(0,t) = \frac{s_i(t)}{l_i + (t-t_i) - (s_i(t) - s_i(t_i))}, \quad y(0,t) = 0. \tag{2.11}$$

Here $s_0(t) = 0$ is the location of the contact point initially.

We consider the formation of a fold as composed of two parts:

(I) the filament becomes tangential to the surface at $t = t_1$ at $x = y = 0$. Further feeding causes the filament to be laid out as the contact point moves to $s = s_1(t)$. The location of the contact point $x(0,t) = s_1(t)$ is then determined by the condition of tangency

$$\phi(s_1(t), t) = 0. \tag{2.12}$$

(II) As the feeding continues past $t = t_1$, the filament begins to dip downwards under its own weight until it touches itself on the horizontal frame for the first time at $t = t_2$, when a second contact point $s_2(t)$ is born. If the filament is being fed slowly, surface tension causes the filament to sinter with the rest of the liquid at this location, i.e. the small rolling motion of the filament can be effectively neglected. Then the part of the fold between $s_2(t)$ and $s_1(t)$ will not move at all and a new contact point moves away from $x = s_2(t)$, with the condition of tangency 2.12 replaced by the new one

$$\phi(s_2(t), t) = \pi. \tag{2.13}$$

After some time the contact line lies directly below the feeding point, thus completing the laying out of half a period of the fold.

2.4 Numerical solution

In the following, we are going to address each of the folding regimes and the computational methods used to simulate them in details.

2.4.1 Regime I

At $t = 0$, the filament touches the horizontal plane and further feeding causes it to buckle, figure 2-4 a). In the presence of friction the point of contact remains fixed, acting as a pivot about which the filament bends.

To proceed with a numerical solution we reformulate the problem in terms of a new variable $\xi = \frac{s}{1+t}$ so an effective length of a curve ξ between the feeding point and the last contact point remains fixed at all times and $0 \leq \xi \leq 1$. Then equations 2.8

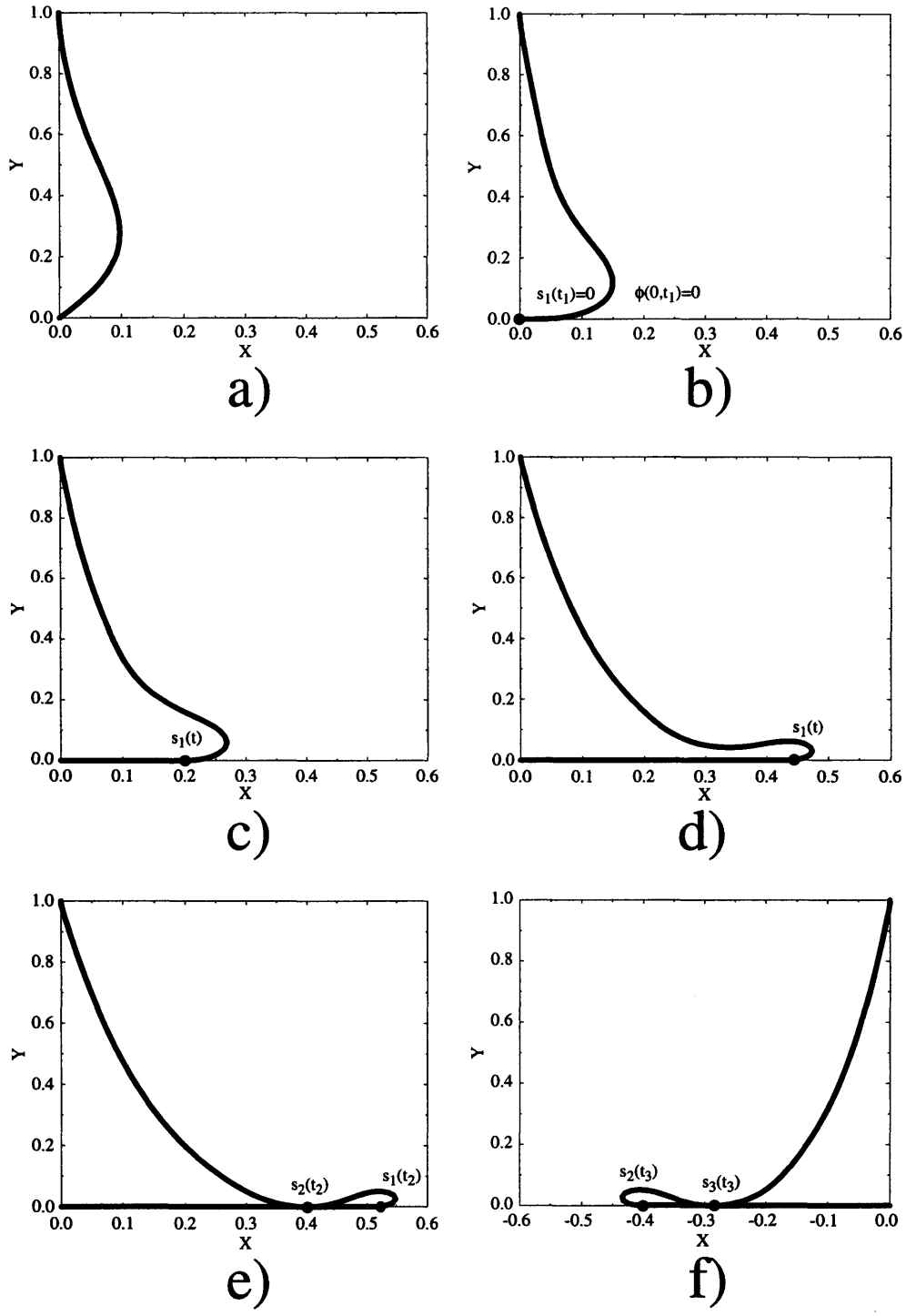

Figure 2-4: a) Regime I of filament folding, $t \leq t_1$. Inflection line pivots around the contact point at $(0,0)$ until $\phi(0,t_1) = 0$. b) At $t = t_1$, inflection line touches the horizontal plane. c) Regime II of filament folding, $t_1 < t \leq t_2$. Contact point $s_1(t)$ moves along x axis away from $(0,0)$. d) As folding in the Regime II proceeds inflection line starts to dip under its own weight toward itself and at $t = t_2$ touches itself for the first time. e) At $t = t_2$, inflection line touches itself for the first time leading to the appearance of the second contact point $s_2(t)$. f) Regime III of filament folding, $t_2 < t \leq t_3$. Contact point $s_2(t)$ is tracing back along x and crossing $(0,0)$ then it reaches its new extremum at $t = t_3$.

transform into

$$\begin{cases} n_{1\xi} &= 0, \\ n_{2\xi} &= (1+t), \\ \eta\phi_{\xi\xi t}(\xi,t) &= \eta\frac{2}{1+t}\phi(\xi,t)_{\xi\xi} + (n_1 sin\phi(\xi,t) - n_2 cos\phi(\xi,t))(1+t)^2. \end{cases} \tag{2.14}$$

The boundary conditions are then

$$\begin{aligned} \phi_\xi(0,t) &= 0, \\ \phi(1,t) &= \tfrac{\pi}{2}, \end{aligned} \tag{2.15}$$

and

$$\begin{aligned} x(0,t) &= 0, \\ x(1,t) &= \textstyle\int_0^1 cos\phi(\xi,t)d\xi \;=\; 0, \\ y(0,t) &= 0, \\ y(1,t) &= \textstyle\int_0^1 sin\phi(\xi,t)d\xi \;=\; \frac{1}{1+t}. \end{aligned} \tag{2.16}$$

For the numerical solution of equations 2.14 we use a finite difference method which exhibits $O(dt^2)$ accuracy in time and $O(d\xi^4)$ in space. Boundary conditions 2.16 are implemented via a relaxation step using a nonlinear damped Newton method, while boundary conditions 2.15 are implemented by choosing a proper form of a finite difference operator $\phi_{\xi\xi}$. Thus, given a solution at time t, a new solution at time $t+dt$ is calculated by using Newton relaxation step subjected to constraints 2.16.

We start time propagation of a solution with a curve close to the $\phi(\xi,0) = \frac{\pi}{2}$. First 3 time steps are implemented with an explicit $O(dt)$, $O(d\xi^4)$ algorithm. Particularly, on a time mesh the finite difference operator is

$$\phi_{\xi\xi}(\xi,t+dt) - \phi_{\xi\xi}(\xi,t) = \frac{2dt}{1+t}\phi_{\xi\xi}(\xi,t) + \frac{dt}{\eta}(n_1(t)sin\phi(\xi,t) - (n_2(t)+\xi(1+t))cos\phi(\xi,t))(1+t)^2. \tag{2.17}$$

All the following steps until $\phi(\xi,t_1)|_{\xi=0} = 0$ are made with an implicit $O(dt^2)$ algorithm where the finite difference operator is

$$\phi_{\xi\xi}(\xi,t+dt)-\phi_{\xi\xi}(\xi,t-dt)=\frac{4dt}{1+t}\phi_{\xi\xi}(\xi,t)+(1+t)^2[$$
$$\frac{dt}{\eta}(n_1(t-dt)sin\phi(\xi,t-dt)-(n_2(t-dt)+\xi(1+t-dt))cos\phi(\xi,t-dt))+ \quad (2.18)$$
$$\frac{dt}{\eta}(n_1(t+dt)sin\phi(\xi,t+dt)-(n_2(t+dt)+\xi(1+t+dt))cos\phi(\xi,t+dt))].$$

To calculate a second order space derivative $\phi_{\xi\xi}$ a spatial mesh of $N+2$ point was used. Equations 2.17, 2.18 were solved on N "inside" points, while the two "outside" points on the edges were used to incorporate the required boundary conditions. Using an equidistant space mesh, points $\xi \in (0,1)$ were represented as a collection of $\xi = (i-1)d\xi$, $i \in 1,...,N$, $d\xi = \frac{1}{N-1}$. Several $O(d\xi^4)$ finite difference operators were used to define $\phi_{\xi\xi}(\xi,t)$ for the N inside points. At the points i, $i \in \{2,...,N-1\}$ a symmetric operator was used

$$\phi_{\xi\xi}(i,t)=\frac{-\frac{1}{12}\phi(i-2,t)+\frac{4}{3}\phi(i-1,t)-\frac{5}{2}\phi(i,t)+\frac{4}{3}\phi(i+1,t)-\frac{1}{12}\phi(i+2,t)}{d\xi^2}+O(d\xi^4), \quad (2.19)$$

while for the points $i \in \{1,N\}$ the assymetric operators were used

$$\phi_{\xi\xi}(1,t)=\frac{\frac{5}{6}\phi(0,t)-\frac{5}{4}\phi(1,t)-\frac{1}{3}\phi(2,t)+\frac{7}{6}\phi(3,t)-\frac{1}{2}\phi(4,t)+\frac{1}{12}\phi(5,t)}{d\xi^2}+O(d\xi^4), \quad (2.20)$$

and

$$\phi_{\xi\xi}(N,t)=-\frac{\frac{5}{6}\phi(N+1,t)-\frac{5}{4}\phi(N,t)-\frac{1}{3}\phi(N-1,t)+\frac{7}{6}\phi(N-2,t)-\frac{1}{2}\phi(N-3,t)+\frac{1}{12}\phi(N-4,t)}{d\xi^2}+O(d\xi^4). \quad (2.21)$$

To incorporate a boundary condition $\phi_\xi(\xi,t)|_{\xi=0} \simeq \phi_\xi(i,t)|_{i=1}=0$ we employ an $O(d\xi^5)$ assymetrical approximation to the derivative at point $i=1$ so that the overall finite difference operator remains $O(d\xi^4)$

$$\phi_\xi(1,t)=\frac{-\frac{1}{5}\phi(0,t)-\frac{13}{12}\phi(1,t)+2\phi(2,t)-\phi(3,t)+\frac{1}{3}\phi(4,t)-\frac{1}{20}\phi(5,t)}{d\xi}+O(d\xi^5). \quad (2.22)$$

As the boundary condition forces $\phi_\xi(\xi,t)|_{\xi=0} \simeq \phi_\xi(i,t)|_{i=1} = 0$ we can eliminate a variable $\phi(0,t)$ from equation 2.20 by expressing it through $\phi(i,t)$, $i \in \{1,2,3,4,5\}$ using equation 2.22. Also, from the second boundary condition we have $\phi(\xi,t)|_{\xi=1} \simeq \phi(i,t)|_{i=N} = \frac{\pi}{2}$. Combining all of the above we now wright the form of the finite difference operator satisfying required boundary conditions 2.15 in a matrix form as following

$$\begin{vmatrix} \phi_{\xi\xi}(1,t) \\ \phi_{\xi\xi}(2,t) \\ \phi_{\xi\xi}(3,t) \\ \phi_{\xi\xi}(4,t) \\ \phi_{\xi\xi}(5,t) \\ \cdots \\ \phi_{\xi\xi}(N-2,t) \\ \phi_{\xi\xi}(N-1,t) \\ \phi_{\xi\xi}(N,t) \end{vmatrix} = \phi(0,t) \begin{vmatrix} \frac{5}{6} \\ -\frac{1}{12} \\ 0 \\ 0 \\ 0 \\ \cdots \\ 0 \\ 0 \\ 0 \end{vmatrix} + \begin{vmatrix} -\frac{5}{4} & -\frac{1}{3} & \frac{7}{6} & -\frac{1}{2} & \frac{1}{12} & & & & \\ \frac{4}{3} & -\frac{5}{2} & \frac{4}{3} & -\frac{1}{12} & & & & & \\ -\frac{1}{12} & \frac{4}{3} & -\frac{5}{2} & \frac{4}{3} & -\frac{1}{12} & & & & \\ & -\frac{1}{12} & \frac{4}{3} & -\frac{5}{2} & \frac{4}{3} & -\frac{1}{12} & & & \\ & & -\frac{1}{12} & \frac{4}{3} & -\frac{5}{2} & \frac{4}{3} & -\frac{1}{12} & & \\ & & & \cdot & \cdot & \cdot & \cdot & \cdot & \\ & & & & -\frac{1}{12} & \frac{4}{3} & -\frac{5}{2} & \frac{4}{3} & 0 \\ & & & & & -\frac{1}{12} & \frac{4}{3} & -\frac{5}{2} & -\frac{1}{12} \\ & & & & \frac{1}{12} & -\frac{1}{2} & \frac{7}{6} & -\frac{1}{3} & \frac{5}{6} \end{vmatrix} \begin{vmatrix} \phi(1,t) \\ \phi(2,t) \\ \phi(3,t) \\ \phi(4,t) \\ \phi(5,t) \\ \cdots \\ \phi(N-2,t) \\ \phi(N-1,t) \\ \phi(N+1,t) \end{vmatrix} + \frac{\pi}{2} \begin{vmatrix} 0 \\ 0 \\ 0 \\ 0 \\ 0 \\ \cdots \\ -\frac{1}{12} \\ \frac{4}{3} \\ -\frac{5}{4} \end{vmatrix} \tag{2.23}$$

where $\phi(0,t)$ is expressed via $\phi(1,t)$, $\phi(2,t)$, $\phi(3,t)$, $\phi(4,t)$, $\phi(5,t)$ by equating 2.22 to zero.

2.4.2 Regime II

At $t = t_1$, the filament becomes tangential to the horizontal plane (see figure 2-4 b)) and the point of contact starts moving away from $x = 0$, figure. 2-4 c). We define $s_1(t)$ to be a position of the first contact point with respect to time. The total length of a filament not touching the horizontal plain will be $(1+t-s_1(t))$. We now reformulate the problem in terms of a new variable $\xi = \frac{s}{1+t-s_1(t)}$ so the length of a curve remains fixed at all times and $0 \leq \xi \leq 1$. Equations 2.8 then transform into

$$\begin{cases} n_{1\xi} &= 0, \\ n_{2\xi} &= (1+t-s_1(t)), \\ \eta\phi_{\xi\xi t}(\xi,t) &= \eta\frac{2(1-s_{1t}(t))}{1+t-s_1(t)}\phi(\xi,t)_{\xi\xi} + (n_1 sin\phi(\xi,t) - n_2 cos\phi(\xi,t))(1+t-s_1(t))^2. \end{cases} \tag{2.24}$$

The boundary conditions are then

$$\begin{aligned} \phi_\xi(0,t) &= 0, \\ \phi(0,t) &= 0, \\ \phi(1,t) &= \tfrac{\pi}{2}, \end{aligned} \tag{2.25}$$

and

$$\begin{aligned} x(0,t) &= s_1(t), \\ x(1,t) &= \tfrac{s_1(t)}{1+t-s_1(t)} + \int_0^1 cos\phi(\xi,t)d\xi = 0, \\ y(0,t) &= 0, \\ y(1,t) &= \int_0^1 sin\phi(\xi,t)d\xi = \tfrac{1}{1+t-s_1(t)}. \end{aligned} \tag{2.26}$$

For numerical solution of equations 2.24 we use a finite difference method which exhibits $O(dt^2)$ accuracy in time and $O(d\xi^4)$ in space. Boundary conditions 2.26 as previously are implemented via a relaxation step using a nonlinear damped Newton method. Thus, given a solution at time t, a new solution at time $t + dt$ is calculated by using Newton relaxation step subjected to constraints 2.26.

Starting with a curve at $t = t_1$, we first make 3 time steps with an explicit $O(dt)$, $O(d\xi^4)$ algorithm. Particularly, on a time mesh the finite difference operator is

$$\begin{aligned} &\phi_{\xi\xi}(\xi,t+dt) - \phi_{\xi\xi}(\xi,t) = \tfrac{2dt(1-s_{1t}(t))}{1+t-s_1(t)}\phi_{\xi\xi}(\xi,t) + \\ &\tfrac{dt}{\eta}(n_1(t)sin\phi(\xi,t) - (n_2(t) + \xi(1+t-s_1(t)))cos\phi(\xi,t))(1+t-s_1(t))^2. \end{aligned} \tag{2.27}$$

All the following steps until the inflection line touches itself at $t = t_2$ are made with an implicit $O(dt^2)$ algorithm where the finite difference operator is

$$\begin{aligned} &\phi_{\xi\xi}(\xi,t+dt) - \phi_{\xi\xi}(\xi,t-dt) = \tfrac{4dt(1-s_{1t}(t)}{1+t-s_1(t)}\phi_{\xi\xi}(\xi,t) + (1+t-s_1(t))^2[\\ &\tfrac{dt}{\eta}(n_1(t-dt)sin\phi(\xi,t-dt) - (n_2(t-dt) + \xi(1+t-dt-(s_1(t)-s_{1t}(t)dt)))cos\phi(\xi,t-dt)) + \\ &\tfrac{dt}{\eta}(n_1(t+dt)sin\phi(\xi,t+dt) - (n_2(t+dt) + \xi(1+t+dt-(s_1(t)+s_{1t}(t)dt)))cos\phi(\xi,t+dt))]. \end{aligned} \tag{2.28}$$

A time derivative $s_{1t}(t)$ of the contact point position $s_1(t)$ is considered explicitly as an unknown variable and $s_1(t + dt)$ is calculated to preserve $O(dt^2)$ accuracy of the method as $s_1(t + dt) = s_1(t - dt) + 2dts_{1t}(t) + O(dt^2)$.

2.4.3 Regime III

As the feeding continues past $t = t_1$ the filament begins to dip downwards under its own weight (see figure 2-4 d)). Finally, the inflection curve touches itself for the first time at $t = t_2$, figure. 2-4 e). The second contact point $s_2(t)$ appears. In practice, because of the surface tension the rest of the curve between $s_2(t)$ and $s_1(t)$ will not move at all and the new boundary conditions at $s_2(t)$ will be the same as in Regime II except for the $\phi(s_2(t), t) = \pi$ rather then $\phi(s_1(t), t) = 0$ as in the Regime II. The same equations as for the Regime II will have to be solved to find a time propagation of a $\phi(s, t)$ field in Regime III where $s_1(t)$ should be substituted by $s_2(t)$. At time $t = t_3$ the filament touches itself for a second time and $t_3 - t_2$ gives half a period of the folding, figure 2-4 f).

2.5 Numerical results

To follow the observed evolution of the viscous fold numerically, we start with an initial condition that is not necessarily consistent with the maximally unstable wavelength of a bending filament. Therefore, we have to wait for several (usually 1-2) complete folds until the influence of the initial conditions disappears and constant periodicity folding is established. To illustrate this point on figure 2-5 we show the evolution of the fold for $\eta = 10^{-4}$.

In figure 2-6 we show the evolution of the contact lines that are formed during each period of the fold for the same value of η. We see that the folding is indeed periodic after a short initial transient associated with the initial conditions.

To check for the predicted scaling laws 2.4 we numerically evaluated the horizontal extent of the fold $L_f(\eta)$ as well as the time period of a stationary fold $T_f(\eta)$ for the various values of η. Calculations were done for a set of $\eta \in \{7 \cdot 10^{-5}, 10^{-4}, 5 \cdot 10^{-4}, 10^{-3}, 5 \cdot 10^{-3}\}$. In figure 2-7, we show a log-log plot of $L_f(\eta)$ and $T_f(\eta))$ vs. η, and see that $log(L_f(\eta)) = B_L log(\eta) + C_L$ and $log(T_f(\eta)) = B_T log(\eta) + C_T$, with $B_L = 0.24 \pm 0.04$, and $B_T = 0.25 \pm 0.04$, which compares very well with the predicted scaling law 2.4.

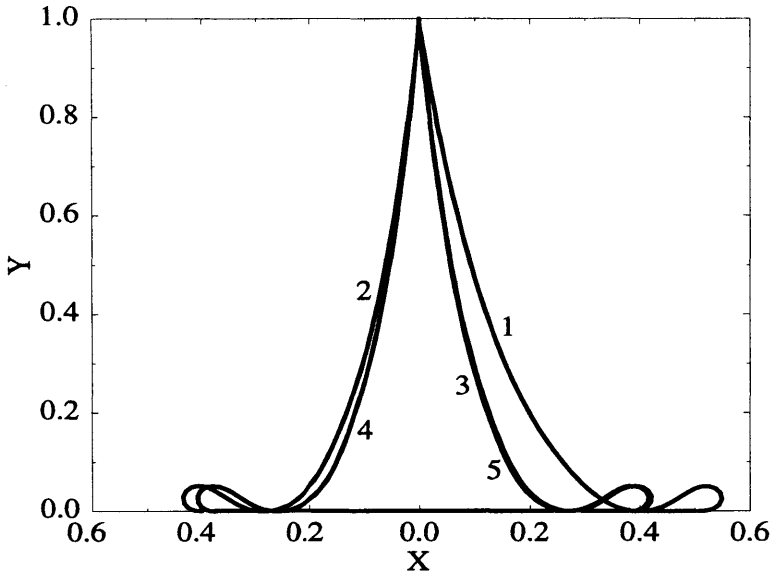

Figure 2-5: Evolution of the fold for $\eta = 10^{-4}$. Memory of initial conditions (half folds 1 and 2) quickly disappears and after the 3rd half a fold, period T_f and the length of a fold L_f remains almost constant.

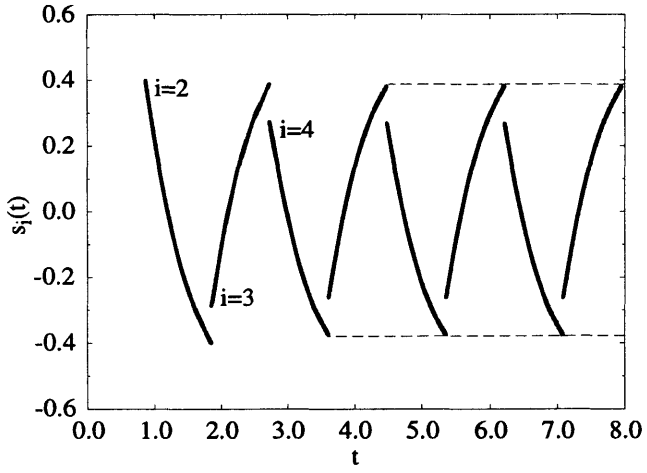

Figure 2-6: The formation and evolution of the contact lines (points) during the folding of the filament. Here, we have assumed that the folds merge with each other over the time scale of the laying of a single fold so that the total fall height remains the same over many periods. $s_i(t)$ denotes the location of the ith contact line; we observe that periodicity is achieved following an initial transient.

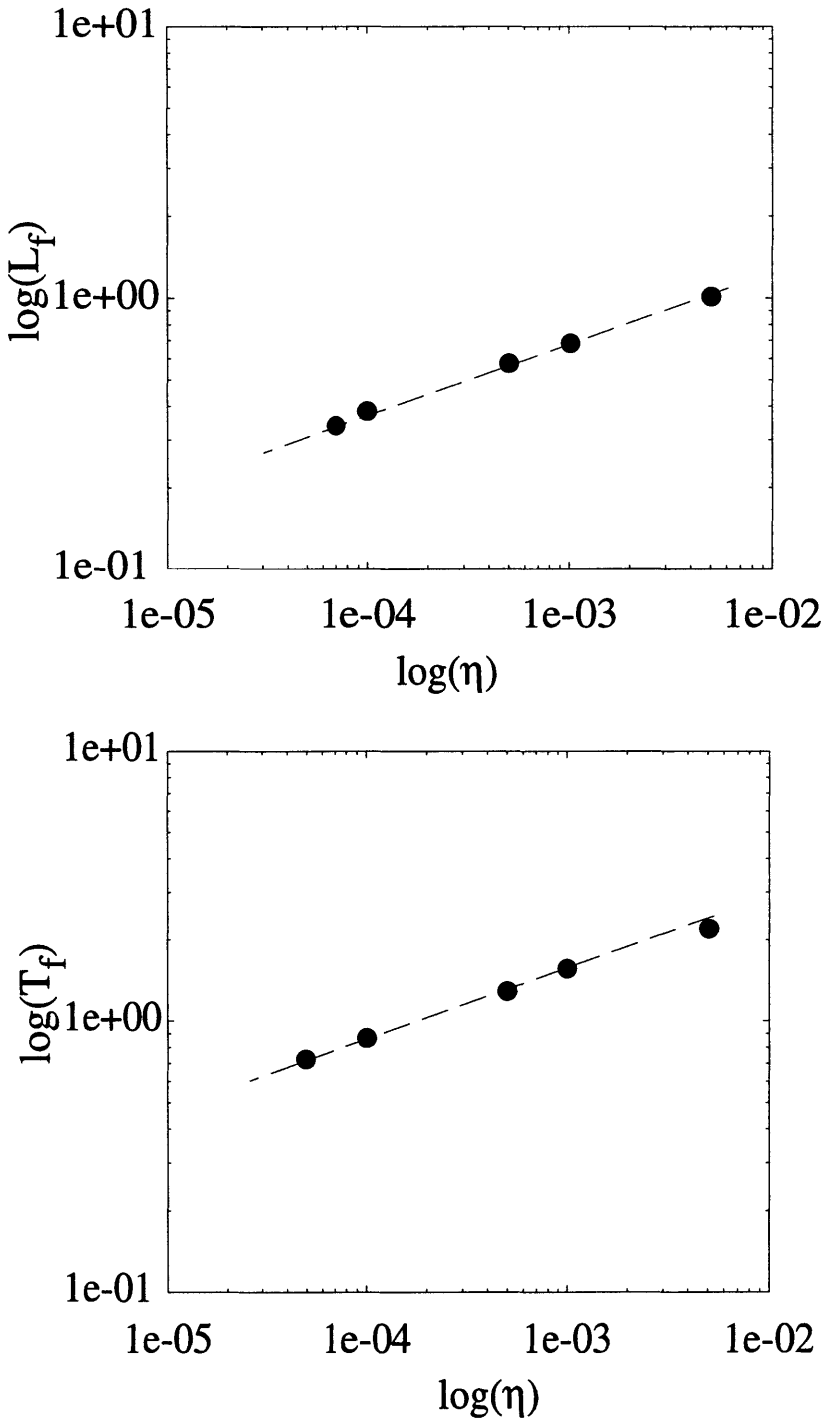

Figure 2-7: (a) The relation between the fold length L_f and η is fitted well by the predicted power law $L_f \sim \eta^{-0.24\pm0.04}$ for $\eta << 1$; (b) The relation between the folding time period T_f and η is fitted well by the predicted power law $T_f \sim \eta^{-0.25\pm0.04}$ for $\eta << 1$.

2.6 Discussion

We conclude with a brief discussion of our results, which have focused on the simplest folding problem for a two-dimensional viscous filament. Using an analogy to the planar bending of elastic sheets, we were able to formulate and solve a free-boundary problem for the periodic folding of viscous filaments. We neglected the effect of the external fluid, and considered only the bending of the filament; stretching playing a role only far from the folding region. The folding of a sheet of constant width and thickness r can be similarly treated by replacing the viscous bending rigidity $3\mu r^4$ of the filament by $\mu r^3/3$ which is the viscous bending rigidity of a sheet per unit width. However, in such cases (see figure 2-1 b)), surface tension causes the lateral edges to come together and necessitates a modification of our theory. For very viscous slow moving sheets, when $\mu v/\sigma >> 1$, such as in geophysical and some materials processing flows, our theory provides a very good starting point in this direction. We have also neglected the effect of the external fluid; this can be remedied by including tangential and normal drag forces that are proportional to the velocity of the filament in the two directions in equation 2.6, while noting the anisotropy of the drag coefficients for slender bodies in a fluid. We are currently addressing this issue in the context of buckling experiments in soap films. On a more general note, just as lubrication-type theories in hydrodynamics assume that the center-line is straight, and look at various modes of the free surface, bending theories assume that the center-line is curved, and look at sinuous modes of the free surface. We believe that there are scores of problems in the hydrodynamics of thin films in this latter regime that can be addressed using these ideas.

Chapter 3

Photon Modes in Photonic Crystals Undergoing Rigid Vibrations

At the end of chapter 1 we have demonstrated how the nature of the electro-magnetic modes in a stationary photonic crystal can be successfully investigated in a planewave basis set, where the problem reduces to a standard eigen value problem. In this chapter we explore the nature of photon modes associated with photonic crystals undergoing rigid time-dependent spatial displacements in a non-inertial frame of reference. We first prove that under certain conditions these modes retain many of the spatial symmetries allowed in a static photonic crystal. Moreover, it is shown quite generally that such non-inertial modes possess a temporal Bloch-like symmetry. Conserved "quantum numbers" are identified and a convenient scheme for labeling non-inertial modes is presented. Computationally, such modes are investigated in a plane-wave basis set. It is shown that finding the spatial and temporal characteristics of such modes is equivalent to solving a generalized eigen value problem of the form

$$(A\omega^2 + B\omega + C)\vec{E} = 0 \tag{3.1}$$

where ω is an eigen value and $\vec{E}$ is an eigen vector. Finally, a method of solution of a generalized eigen value problem based on nonlinear Newton iterations is proposed.

The idea of using periodic dielectric materials (photonic crystals) to alter the dispersion relation of photons [12, 13, 14] has received widespread interest and consideration because of numerous potential applications [15]. It has been shown by several authors [15, 16, 17, 18] that passive elements such as waveguide bends, channel drop filters, mirror surfaces, etc. can be substantially improved if constructed on the basis of photonic crystals. Recently, a strong interest has developed for the incorporation of non-linear materials into photonic crystals. Investigations in the framework of field-dependent dielectric media have led to several suggestions [19, 20, 21] on the possibility of constructing active elements such as optical switches, and on the realization of dynamical effects such as second-harmonic generation and induced inter-band transitions in photonic crystals. In all of these studies, the photonic crystals are constrained to be in a static, or inertial, frame of reference. Nevertheless, it should be possible to develop active photonic crystal elements even with *linear* materials by working with *non-stationary* photonic crystals. Before one can begin to explore this possibility it is necessary to have a fundamental framework of understanding of the nature of the photonic states in such non-inertial systems.

In the following we explore the properties of photon modes associated with photonic crystals undergoing rigid time-dependent spatial vibrations in the non-relativistic limit. A fundamental theorem about the form of the resulting electro-magnetic modes in a non-inertial frame is presented. Specifically, we prove that photonic crystals undergoing such rigid displacements can exhibit solutions that, under certain circumstances, exhibit Bloch-like spatial and temporal translational symmetries. To our knowledge, this is the first time photonic crystals have been investigated in a non-inertial frame of reference.

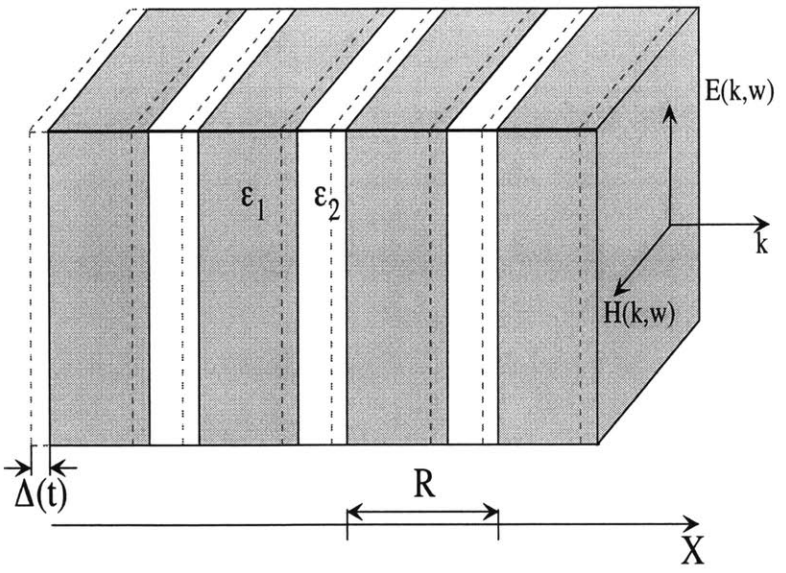

Figure 3-1: 1D photonic crystal with periodicity R rigidly translated with a displacement $\triangle(t)$.

3.1 Theoretical formulation

Let us now consider a photonic crystal rigidly vibrating with an amplitude Δ and a driving frequency Ω as illustrated in figure 3-1, where R is the periodicity of a photonic crystal and R_1, R_2 are the widths of the slabs with dielectric constants ϵ_1 and ϵ_2 consequently.

In this case Maxwell's equations take the form

$$\begin{cases} \bigtriangledown \times H(\vec{r},t) &= \epsilon(\vec{r}-\vec{\Delta}(t))\frac{\partial E(\vec{r},t))}{c\partial t} + \frac{\partial \epsilon(\vec{r}-\vec{\Delta}(t))}{c\partial t}E(\vec{r},t) \\ \bigtriangledown \times E(\vec{r},t) &= -\frac{\partial H(\vec{r},t)}{c\partial t} \end{cases} \tag{3.2}$$

where $\epsilon(\vec{r},t)$ is a spatially periodic time dependent function such that there exists $\vec{R}$ so that for all $\vec{r}$: $\epsilon(\vec{r}+\vec{R}-\vec{\Delta}(t)) = \epsilon(\vec{r}-\vec{\Delta}(t))$ and $\vec{\Delta}(t) = \vec{\Delta}(t+\frac{2\pi}{\Omega})$. We now prove that a Bloch-like symmetry of non-stationary modes still holds in the non-inertial case.

To prove this statement we search for a solution to the non-inertial problem in a

complete plain wave basis

$$\begin{pmatrix} H(\vec{r},t) \\ E(\vec{r},t) \end{pmatrix} = \int d\vec{k}d\omega \begin{pmatrix} H(\vec{k},\omega) \\ E(\vec{k},\omega) \end{pmatrix} |\vec{k},\omega>, \tag{3.3}$$

where we define $|\vec{k},\omega>=\frac{1}{(2\pi)^2}\exp(i\vec{k}\cdot\vec{r}-i\omega t)$ and $<\vec{k}_0,\omega_0|\vec{k},\omega>=\delta(\vec{k}_0-\vec{k})\delta(\omega_0-\omega)$.

Substituting equation 3.3 into Maxwell's equations 3.2 and multiplying both sides by $\frac{1}{i}<\vec{k}_0,\omega_0|$ we obtain

$$\begin{cases} 0 &= H(\vec{k}_0,\omega_0)\times\vec{k}_0 - \int d\vec{k}d\omega\frac{\omega}{c}E(\vec{k},\omega)<\vec{k}_0,\omega_0|\epsilon(\vec{r}-\vec{\Delta}(t))|\vec{k},\omega> - \\ & \quad i\int d\vec{k}d\omega E(\vec{k},\omega)<\vec{k}_0,\omega_0|\frac{\partial\epsilon(\vec{r}-\vec{\Delta}(t))}{c\partial t}|\vec{k},\omega> \\ 0 &= E(\vec{k}_0,\omega_0)\times\vec{k}_0+\frac{\omega_0}{c}H(\vec{k}_0,\omega_0). \end{cases} \tag{3.4}$$

We now proceed to evaluate the integrals over the wavevector space in equation 3.4. Since $\epsilon(\vec{r}+\vec{R})=\epsilon(\vec{r})$ we can represent a dielectric function in the reciprocal vector space as $\epsilon(\vec{r})=\sum_{\vec{G}}\epsilon_{\vec{G}}\exp(i\vec{G}\cdot\vec{r})$. Substituting this representation of $\epsilon(\vec{r})$ into equation 3.4 the first integral can be written

$$\int d\vec{k}d\omega\frac{\omega}{c}E(\vec{k},\omega)<\vec{k}_0,\omega_0|\epsilon(\vec{r}-\vec{\Delta}(t))|\vec{k},\omega>=$$
$$\int d\vec{k}d\omega\frac{\omega}{c}E(\vec{k},\omega)\sum_{\vec{G}}\epsilon_{\vec{G}}<k_0,\omega_0|\exp(i\vec{G}\cdot\vec{r}-i\vec{G}\cdot\vec{\Delta}(t))|\vec{k},\omega>. \tag{3.5}$$

Now the spatial part of the matrix element can be trivially calculated to give

$$<\vec{k}_0,\omega_0|\exp(i\vec{G}\cdot\vec{r}-i\vec{G}\cdot\vec{\Delta}(t))|\vec{k},\omega>=\delta(\vec{k}+\vec{G}-\vec{k}_0)\frac{1}{2\pi}\int dt\exp(i(\omega_0-\omega)t-i\vec{G}\cdot\vec{\Delta}(t)). \tag{3.6}$$

Since $\vec{\Delta}(t)$ is a periodic function of time with period $\frac{2\pi}{\Omega}$, the integral over time can be rewritten in the following way

$$\frac{1}{2\pi}\int dt\exp\left(i(\omega_0-\omega)t-i\vec{G}\cdot\vec{\Delta}(t)\right)=\left(\sum_{l=-\infty}^{+\infty}\exp\left(i(\omega_0-\omega)\frac{2\pi}{\Omega}l\right)\right)\frac{1}{2\pi}\int_0^{\frac{2\pi}{\Omega}}dt\exp\left(i(\omega_0-\omega)t-i\vec{G}\cdot\vec{\Delta}(t)\right). \tag{3.7}$$

Using the identity $\sum_{l=-\infty}^{+\infty} \exp\left(i(\omega_0-\omega)\frac{2\pi}{\Omega}l\right) = \Omega\sum_{l=-\infty}^{+\infty}\delta(\omega-(\omega_0+l\Omega))$ one finally arrives at

$$\int d\vec{k}d\omega\frac{\omega}{c}E(\vec{k},\omega) < k_0,\omega_0|\epsilon(\vec{r}-\vec{\Delta}(t))|\vec{k},\omega >=$$
$$\frac{1}{c}\sum_{\vec{G}}\epsilon_{\vec{G}}\sum_{l=-\infty}^{+\infty}E(\vec{k}_0-\vec{G},\omega_0+l\Omega)(\omega_0+l\Omega)\frac{\Omega}{2\pi}\int_0^{\frac{2\pi}{\Omega}}dt\exp\left(-i\vec{G}\cdot\vec{\Delta}(t)-il\Omega t\right). \quad (3.8)$$

Proceeding in exactly the same fashion, the second integral in equation 3.4 can be manipulated to give

$$i\int d\vec{k}d\omega E(\vec{k},\omega) < \vec{k}_0,\omega_0|\frac{\partial\epsilon(\vec{r}-\vec{\Delta}(t))}{c\partial t}|\vec{k},\omega >=$$
$$-\frac{1}{c}\sum_{\vec{G}}\epsilon_{\vec{G}}\sum_{n=-\infty}^{+\infty}E(\vec{k}_0-\vec{G},\omega_0+l\Omega)l\Omega\frac{\Omega}{2\pi}\int_0^{\frac{2\pi}{\Omega}}dt\exp\left(-i\vec{G}\cdot\vec{\Delta}(t)-il\Omega t\right). \quad (3.9)$$

Combining the results above, we arrive at the following form of Maxwell's equations in the wavevector representation.

$$\begin{cases} 0 &= H(\vec{k}_0,\omega_0)\times\vec{k_0}-\frac{\omega_0}{c}\sum_{\vec{G}}\epsilon_{\vec{G}}\sum_{l=-\infty}^{+\infty}E(\vec{k}_0-\vec{G},\omega_0+l\Omega)\frac{\Omega}{2\pi}\int_0^{\frac{2\pi}{\Omega}}dt\exp\left(-i\vec{G}\cdot\vec{\Delta}(t)-il\Omega t\right) \\ 0 &= E(\vec{k}_0,\omega_0)\times\vec{k_0}+\frac{\omega_0}{c}H(\vec{k}_0,\omega_0). \end{cases} \quad (3.10)$$

There are three immediate conclusions that can be drawn from the form of equation 3.10. First, modes with different $\vec{k}_0$ within the conventional Brillouin zone do not mix so that it is still possible to define a "good" quantum number $\vec{k}_0$ for a vibrating photonic crystal, regardless of the direction of vibration. In passing we note that for a 1D or 2D periodic photonic crystal, if one chooses a vector of vibration $\vec{\Delta}$ perpendicular to the reciprocal vector space of the structure, only the $l=0$ term survives in equation 3.10 and the problem reduces (in non-relativistic limit) to that of the static case.

Secondly, for a given mode with a native band frequency ω_0 and amplitude $\begin{pmatrix} H(\vec{k}_0,\omega_0) \\ E(\vec{k}_0,\omega_0) \end{pmatrix}$, the harmonics with the satellite frequencies $\omega_0+l\Omega$ and amplitudes

$\begin{pmatrix} H(\vec{k}_0, \omega_0 + l\Omega) \\ E(\vec{k}_0, \omega_0 + l\Omega) \end{pmatrix}$ are also present. And finally, for a given $\vec{k}_0$ there will be a discrete set of $\omega_{0,n}$'s which satisfy equation 3.10. These $\omega_{0,n}$'s are analogous to the photon bands of the static photonic crystal.

In general therefore, any time dependent solution $\begin{pmatrix} H_\Omega(\vec{r}, t) \\ E_\Omega(\vec{r}, t) \end{pmatrix}$ of equation 3.2 can be expressed in a basis set of non-inertial modes each satisfying equation 3.2 and characterized by a set of "good" quantum numbers $\vec{k}$ and ω_n so that

$$\begin{pmatrix} H_{\vec{k},\omega_n,\Omega}(\vec{r}, t) \\ E_{\vec{k},\omega_n,\Omega}(\vec{r}, t) \end{pmatrix} = \sum_{\vec{G}} \sum_{l=-\infty}^{+\infty} \begin{pmatrix} H(\vec{k} - \vec{G}, \omega_n + l\Omega) \\ E(\vec{k} - \vec{G}, \omega_n + l\Omega) \end{pmatrix} \exp(i(\vec{k} - \vec{G}) \cdot \vec{r} - i(\omega_n + l\Omega)t). \tag{3.11}$$

It is straightforward to see that such modes possess a spatial and temporal Bloch symmetry

$$\begin{pmatrix} H_{\vec{k},\Omega,\omega_n}(\vec{r} + \vec{R}, t + \frac{2\pi}{\Omega}) \\ E_{\vec{k},\Omega,\omega_n}(\vec{r} + \vec{R}, t + \frac{2\pi}{\Omega}) \end{pmatrix} = \exp(i\vec{k} \cdot \vec{R} - i\omega_n \frac{2\pi}{\Omega}) \begin{pmatrix} H_{\vec{k},\Omega,\omega_n}(\vec{r}, t) \\ E_{\vec{k},\Omega,\omega_n}(\vec{r}, t) \end{pmatrix}. \tag{3.12}$$

3.2 General form of the electro-magnetic modes of a vibrating photonic crystal

For the vibration scenario the $\omega_n(\Omega)$ spectrum will generally be rather complex. To illustrate what this spectrum will typically consists of consider the following argument. Since changing $\omega_n(\Omega)$ to $\omega_n(\Omega) + l\Omega$ for any integer l leads to the same state (see equation 3.11), all the labels $\omega_n(\Omega)$ can be mapped trivially to the interval $[-\frac{\Omega}{2}, \frac{\Omega}{2}]$. For any proper choice of wavevector, each corresponding $\omega_n(\Omega)$ will be a band of modes as sketched in figure 3-2.

Since plotting a complete band structure is very involved, it is instructive to illustrate a simple case where we only have two bands and where coupling between the modes is very weak (that corresponds to $\frac{\Delta\Omega}{c} \to 0$ for vibrations and $\frac{L\Omega}{c} \to 0$ for rotations). Under these conditions the frequencies of the bands folded into the

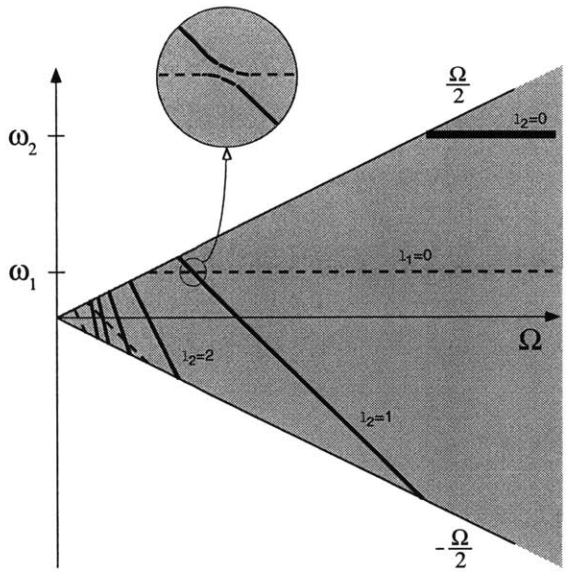

Figure 3-2: Non-inertial band structure as a function of driving frequency Ω is presented for a case of two non-stationary modes. For each value of Ω the frequencies of the bands $\omega_{1,2}(\Omega) \approx \omega_{1,2}(0) + l_{1,2}\Omega$ are mapped into the interval $[-\frac{\Omega}{2}, \frac{\Omega}{2}]$. For a set of driving frequencies $\Omega = \frac{\omega_2 - \omega_1}{l}$ bands will exhibit a near crossing as shown in the insert.

interval $[-\frac{\Omega}{2}, \frac{\Omega}{2}]$, $\omega_n(\Omega)$, will correspond approximately to $\omega_n(\Omega) \simeq \omega_n(0) + l\Omega$ over the whole range of a driving frequency Ω. For a special set of driving frequencies $\Omega = \frac{\omega_2 - \omega_1}{l}$, bands of the same symmetry will exhibit a near crossing (insert on figure 3-2). The amplitude of this splitting will be proportional to the coupling parameter and will become vanishingly small as the value of l increases. In practice, therefore the major splitting will occur at the primary inter-band resonant frequency $\Omega \sim \omega_2 - \omega_1$. The approach described above can, of course, be readily generalized to include more bands. Finally, we conclude with the observation that in the weak coupling limit it can be shown that a possibility exists of using vibrations and rotations to induce inter-band transitions between the photon crystal modes in a novel and controlled fashion without the necessity of employing non-linear materials.

3.3 Numerical computation of the electro-magnetic modes of a vibrating photonic crystal

In this section we outline a method for a computational evaluation of the electro-magnetic modes of a vibrating photonic crystal. As it was shown above, such modes are characterized by a wavevector $\vec{k}$ and a set of frequencies $\omega_n(\Omega)$ and in a planewave basis set they can be written as

$$\begin{pmatrix} H_{\vec{k},\omega_n,\Omega}(\vec{r},t) \\ E_{\vec{k},\omega_n,\Omega}(\vec{r},t) \end{pmatrix} = \sum_{\vec{G}} \sum_{l=-\infty}^{+\infty} \begin{pmatrix} H(\vec{k}-\vec{G},\omega_n+l\Omega) \\ E(\vec{k}-\vec{G},\omega_n+l\Omega) \end{pmatrix} \exp(i(\vec{k}-\vec{G})\cdot\vec{r} - i(\omega_n+l\Omega)t) \tag{3.13}$$

where a set of coefficients $\begin{pmatrix} H(\vec{k}-\vec{G},\omega_n+l\Omega) \\ E(\vec{k}-\vec{G},\omega_n+l\Omega) \end{pmatrix}$ is determined by the equations

$$\begin{cases} 0 &= H(\vec{k},\omega)\times\vec{k} - \frac{\omega}{c}\sum_{\vec{G}}\epsilon_{\vec{G}}\sum_{l=-\infty}^{+\infty} E(\vec{k}-\vec{G},\omega+l\Omega)\frac{\Omega}{2\pi}\int_0^{\frac{2\pi}{\Omega}} dt \exp\left(-i\vec{G}\cdot\vec{\Delta}(t) - il\Omega t\right) \\ 0 &= E(\vec{k},\omega)\times\vec{k} + \frac{\omega}{c}H(\vec{k},\omega). \end{cases} \tag{3.14}$$

As we have seen in chapter one an analogous set of equations for a stationary photonic crystal constitutes an eigen value problem with respect to the frequencies of the electro-magnetic modes. In the following we show that equation 3.14 can be thought of as a generalized eigen value problem that can be solved numerically by nonlinear Newton method starting with the solutions for the electro-magnetic modes of a stationary photonic crystal.

In all that follows we deal with a one dimensional photonic crystal (see figure 3-1). First, let us substitute the second of the equations 3.14 into the first one which leads to an equivalent set of equations

$$\begin{cases} E(k,\omega_n)k^2 &= \frac{\omega_n^2}{c^2}\sum_G \epsilon_G \sum_{l=-\infty}^{+\infty} A(G,l)E(k-G,\omega_n+l\Omega) \\ H(k,\omega_n) &= \frac{ck}{\omega_n}E(k,\omega_n) \end{cases} \tag{3.15}$$

where $A(G,l)$ is defined as

$$A(G,l) = \frac{\Omega}{2\pi}\int_0^{\frac{2\pi}{\Omega}} dt \exp\left(-iG\Delta(t) - il\Omega t\right) = \int_0^1 d\xi \exp\left(-iG\Delta(\xi) - i2\pi l\xi\right). \quad (3.16)$$

Computationally, we restrict the choices of G vectors and the higher harmonics l used in equation 3.15 to be such that $|G| \leq \frac{2\pi}{R}N$ and $|l| < L$. Clearly, solution for the electric field will provide all the necessary information for finding a magnetic field using the second of the equations 3.15. Redefining $G = \frac{2\pi}{R}$, a vector of unknowns to be solved for is then

$$\left|\begin{array}{c} E(k+NG,\omega_n+L\Omega) \\ E(k+NG,\omega_n+(L-1)\Omega) \\ \cdots \\ E(k+NG,\omega_n) \\ \cdots \\ E(k+NG,\omega_n-(L-1)\Omega) \\ E(k+NG,\omega_n-L\Omega) \\ \cdots \\ \cdots \\ \cdots \\ E(k,\omega_n+L\Omega) \\ E(k,\omega_n+(L-1)\Omega) \\ \cdots \\ E(k,\omega_n) \\ \cdots \\ E(k,\omega_n-(L-1)\Omega) \\ E(k,\omega_n-L\Omega) \\ \cdots \\ \cdots \\ \cdots \\ E(k-NG,\omega_n+L\Omega) \\ E(k-NG,\omega_n+(L-1)\Omega) \\ \cdots \\ E(k-NG,\omega_n) \\ \cdots \\ E(k-NG,\omega_n-(L-1)\Omega) \\ E(k-NG,\omega_n-L\Omega) \end{array}\right| . \quad (3.17)$$

To simplify notation we define

$$\vec{E}(k) = \left| \begin{array}{c} E(k, \omega_n + L\Omega) \\ E(k, \omega_n + (L-1)\Omega) \\ \cdots \\ E(k, \omega_n) \\ \cdots \\ E(k, \omega_n - (L-1)\Omega) \\ E(k, \omega_n - L\Omega) \end{array} \right| \tag{3.18}$$

then vector 3.17 can be written as

$$\left| \begin{array}{c} \vec{E}(k + NG) \\ \vec{E}(k + (N-1)G) \\ \cdots \\ \vec{E}(k) \\ \cdots \\ \vec{E}(k - (N-1)G) \\ \vec{E}(k - NG) \end{array} \right| . \tag{3.19}$$

We also define matrixes $A(iG)$ and $D(k, \omega, iG)$ as

$$A(iG) = \begin{pmatrix} A(iG,0) & A(iG,1) & \cdot & A(iG,L) & & & \\ A(iG,-1) & A(iG,0) & \cdot & A(iG,L-1) & A(iG,L) & & \\ \cdot & \cdot & \cdot & \cdot & \cdot & \cdot & \cdot \\ A(iG,-L) & \cdot & A(iG,-1) & A(iG,0) & A(iG,1) & \cdot & A(iG,L) \\ \cdot & \cdot & \cdot & \cdot & \cdot & \cdot & \cdot \\ & & A(iG,L) & \cdot & A(iG,-1) & A(iG,0) & A(iG,1) \\ & & & A(iG,L) & \cdot & A(iG,-1) & A(iG,0) \end{pmatrix}, \tag{3.20}$$

$$D(k,\omega,iG) = \begin{pmatrix} \frac{(\omega+L\Omega)^2}{(k+iG)^2} & & & & & \\ & \frac{(\omega+(L-1)\Omega)^2}{(k+iG)^2} & & & & \\ & & \cdot & & & \\ & & & \frac{\omega^2}{(k+iG)^2} & & \\ & & & & \cdot & \\ & & & & & \frac{(\omega-L\Omega)^2}{(k+iG)^2} \end{pmatrix}. \quad (3.21)$$

Finally, after a number of simple manipulations equation 3.15 can be written in a matrix form as

$$\begin{vmatrix} \vec{E}(k+NG) \\ \cdot \\ \vec{E}(k) \\ \cdot \\ \vec{E}(k-NG) \end{vmatrix} = \frac{1}{c^2} \begin{pmatrix} D(k,\omega,NG) & & & \\ & \cdot & & \\ & & D(k,\omega,0) & \\ & & & \cdot \\ & & & D(k,\omega,-NG) \end{pmatrix} \begin{pmatrix} \epsilon_0 A(0) & \cdot & \epsilon_{NG} A(NG) & & \\ \epsilon_{-G} A(-G) & \epsilon_0 A(0) & \cdot & \epsilon_{NG} A(NG) & \\ \cdot & \cdot & \epsilon_0 A(0) & \cdot & \cdot \\ & \epsilon_{-NG} A(-NG) & \cdot & \epsilon_0 A(0) & \epsilon_G A(G) \\ & & \epsilon_{-NG} A(-NG) & \cdot & \epsilon_0 A(0) \end{pmatrix} \begin{vmatrix} \vec{E}(k+NG) \\ \cdot \\ \vec{E}(k) \\ \cdot \\ \vec{E}(k-NG) \end{vmatrix} \quad (3.22)$$

If an amplitude of the vibrations Δ goes to 0 then it can be seen from the form of the matrices $D(k,\omega,iG)$ and $A(iG)$ that equation 3.22 reduces to an eigen value problem where a set of the eigen frequencies ω_n and a set of the eigenvectors 3.17 become the same as in chapter one equation 1.40. For $\Delta \neq 0$ the matrix form of the equations 3.15 represents a generalized eigen value problem where eigenvalues do not enter the equations in a usual linear way but rather through a matrix $D(k,\omega,iG)$.

To solve a generalized eigen value problem 3.22 we first notice that in a case of a vibrating photonic crystal the perturbation parameter scales as $\frac{\Delta\Omega}{c}$. Defining $\eta = \frac{\Delta\Omega}{c}$ and for the realistic velocities of vibration $\Delta\Omega \leq 100\frac{m}{sec}$, η turns out to be very small and is on the order of 10^{-7}. Thus, one would expect that a solution to a problem of a vibrating photonic crystal in terms of the band structure ω_n and components of the electric field 3.17 should be close to a solution for a stationary photonic crystal. Particularly, the splitting between the bands with frequencies ω_1, ω_2 while in resonance at driving frequency $\Omega = (\omega_2 - \omega_1)$ is also expected to be small and scale as $\eta\Omega$. From these considerations we can employ a nonlinear Newton

method to solve (3.22) with a starting point at frequencies and field components that of a non-stationary photonic crystal.

To proceed with nonlinear Newton method we need to introduce one extra equation. System 3.22 provides $(2N+1)(2L+1)$ equations for $(2N+1)(2L+1)+1$ unknowns ($(2N+1)(2L+1)$ components of an electric field and 1 unknown frequency ω). To compliment equation 3.22 we consider a constraint on the form of the modes such that for any eigenvector 3.17 its norm is constant and equal to 1. This constraint is somewhat arbitrary but it is convenient as a renormalization of the eigenvectors does not change the corresponding eigenvalues.

Finally, we present a solution of equation 3.22 for a one dimensional photonic crystal (see figure 3-1) where $R=1$, $\epsilon(x)=1.5+0.5cos(\frac{2\pi}{R}x)$, $\Delta(t)=0.001Rsin(\Omega t)$ and the maximum numbers of the G vectors and higher harmonics l used are $N=5$, $L=5$. Coupling constant for this system is, therefore, on the order of 10^{-3}. Driving frequency Ω is taken to be a resonant frequency between the first and the second stationary bands $\Omega=(\omega_2-\omega_1)$. We concentrate on the behavior of the bands near the crossover regime as sketched on the insert of figure 3-2. Computed frequencies of the non-stationary bands in the resonance region are shown on figure 3-3. Solid lines on that figure correspond to the band frequencies of the non-interacting bands (in a folded representation). These lines cross at the resonance frequency $\Omega=(\omega_2-\omega_1)$. Circles on figure 3-3 correspond to the frequencies of the non-stationary bands. It is clearly seen that non-stationary bands in a resonance regime exhibit avoiding crossing with the band frequency splitting, as expected, on the order of a coupling constant.

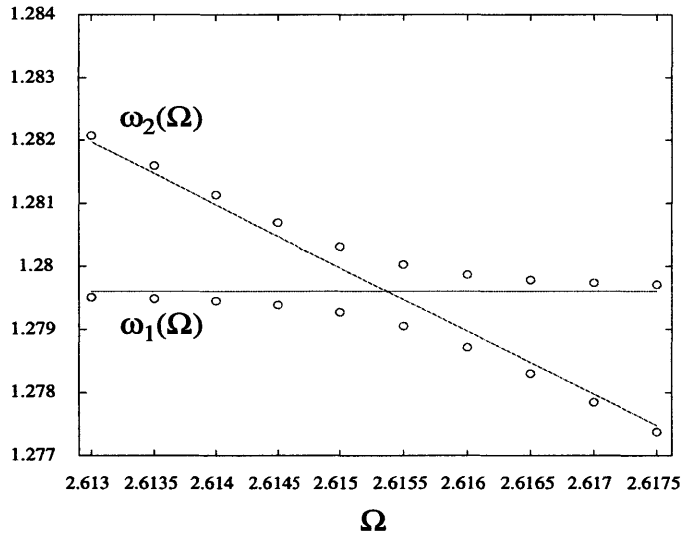

Figure 3-3: Frequencies of the stationary modes are plotted as solid lines while frequencies of the non-stationary modes are plotted in circles. As seen from the plot, non-stationary bands in a resonance regime exhibit avoiding crossing with the band splitting on the order of a coupling constant $\eta = 10^{-3}$.

Bibliography

[1] W.H. Press, B.P. Flannery, S.A. Teukolsky, and W.T. Vetterling. *Numerical Recipies, the Art of Scientific Computing.* Cambridge University Press, 1986.

[2] B. Fornberg and D. Sloan. *A review of pseudospectral methods of solving partial differential Equations.* in Acta Numerica, Cambridge University Press, 1994.

[3] T. A. Arias. Multiresolution analysis of electronic structure: semicardinal and wavelet bases. *Reviews of Modern Physics*, 71:267–312, 1999.

[4] G. I. Taylor. *Proc. 12th Int. Conf. on Applied Mechanics*, pages 382–395, 1969.

[5] A.M. Johnson and Fletcher. *Folding of Viscous Layers.* Columbia University Press, 1994.

[6] S. Chandrasekhar. *Liquid Crystals.* Columbia University Press, 1992.

[7] L. Mahadevan, W. Ryu, and A. Samuel. *Nature*, 392:140, 1998.

[8] L. Mahadevan and J.B. Keller. *SIAM J. App. Math.*, 55:1609–24, 1995.

[9] A.L. Yarin. *J. Fluid Mech.*, 260, 1996.

[10] L. Landau and E.M. Lifshitz. *Theory of Elasticity.* Pergamon Press, 1989.

[11] J. Buckmaster. *J. Fluid Mech.*, 25, 1971.

[12] E. Yablonovich. *Phys. Rev. Lett.*, 58:1059, 1987.

[13] S. John. *Phys. Rev. Lett.*, 58:2486, 1987.

[14] J.D. Joannopoulos, R.D. Meade, and J. N. Winn. *Photonic Crystals.* Princeton University Press, 1995.

[15] *See, e.g., Proc. of Int. Workshop on Electromagnetic Crystal Structures, Laguna Beach, CA (1998) in IEEE Transactions on Microwave Theory and Techniques,* 1999.

[16] A. Mekis *et al. Phys. Rev. B,* 58:4809, 1998.

[17] S. Fan *et al. Phys. Rev. Lett.*, 80:960, 1998.

[18] J. N. Winn *et al. Optics Letters*, 23:1573, 1998.

[19] P. Tran. *Phys. Rev. Lett.*, 21:1138, 1996.

[20] J. Martorell *et al. Appl. Phys. Lett.*, 70:702, 1997.

[21] J. N. Winn *et al. Phys. Rev. B,* 59:1551, 1999.